Increased abyssal ocean density stratification across the Middle Pleistocene Transition

Nicola C. Thomas[1], Heather L. Ford[2], Mervyn Greaves[1], and David A. Hodell[1]

[1]Godwin Laboratory for Palaeoclimate Research, Department of Earth Sciences, University of Cambridge; Cambridge, CB2 3EQ, UK
[2]School of Geography, Queen Mary University of London; London, E1 4NS, UK

Correspondence: Nicola C. Thomas (nct30@cam.ac.uk ; nct3051@gmail.com)

Abstract. We report basin-scale and globally distributed compilations of deep-water temperature and $\delta^{18}O_{seawater}$ for the past 1.5 million years using paired oxygen isotopic ($\delta^{18}O$) and Mg/Ca measurements of benthic foraminifera. Across the Middle Pleistocene Transition (MPT), interbasinal gradients suggest North Atlantic deep-water became colder while Pacific deep-water became more saline during glacial periods after ~930 thousand years ago (ka). The $\delta^{18}O$ of seawater increased in both the deep Atlantic and Pacific across the MPT indicating increased continental ice volume. But the increase was greater in the Pacific than the Atlantic, which we suggest represents increased salinity of Southern Component Water (SCW). We propose the following sequence of changes during the MPT as a working hypothesis: (1) freshwater input to the marginal seas around Antarctica was reduced beginning at 930 ka by decreased melting of the Antarctic Ice Sheet and/or marine ice shelves and increased sea ice formation in the Southern Ocean; (2) the salinity and density of SCW increased, resulting in enhanced abyssal stratification and rendering the deep ocean a more effective carbon trap; (3) together with increased export production of organic matter and reduced deep-to-surface water exchange in the Southern Ocean, carbon storage in the deep ocean increased, lowering glacial atmospheric pCO_2; (4) lower pCO_2 permitted the growth of larger continental ice sheets, which reached a critical size and lengthened the glacial cycles. Our hypothesis supports an important role for abyssal ocean stratification in the MPT, and requires further testing with additional benthic Mg/Ca-$\delta^{18}O$ records, numerical model simulations, and forthcoming atmospheric pCO_2 and mean ocean temperature results from the Beyond EPICA–Oldest Ice core from Antarctica.

1 Introduction

The Middle Pleistocene Transition (MPT), which occurred between ~1.25 and 0.64 million years ago (Ma), marks a major reorganisation of the global climate system and remains a central topic of palaeoclimate research since its first recognition over 50 years ago (Shackleton and Opdyke, 1976). Benthic foraminiferal oxygen isotope ($\delta^{18}O$) records are marked by a shift from dominant 41 thousand year (kyr) to quasi-100 kyr glacial-interglacial cycles across the MPT. There was no commensurate change in orbital forcing (Clark et al., 2006; Pisias and Moore, 1981), suggesting processes internal to the climate system were responsible. The exact cause(s) of the MPT remain(s) an open question (see reviews by (Berends et al., 2021a; Clark et al., 2006; Herbert, 2023; McClymont et al., 2013)). Uncertainties include whether the transition was gradual or abrupt (Sosdian and Rosenthal, 2009; Elderfield *et al.*, 2012; Ford *et al.*, 2016; Legrain, Parrenin and Capron, 2023) and whether it was driven primarily by Northern or Southern Hemisphere processes (An et al., 2024; Basak et al., 2026; Hines et al., 2024; Pérez-Montero et al., 2026; Starr et al., 2021; Williams et al., 2024; Wirths et al., 2025; Yehudai et al., 2021). Most hypotheses invoke a long-term global cooling, commonly attributed to a reduction in atmospheric carbon dioxide (pCO_2) (Berends et al., 2021a; Clark et al., 2006; Willeit et al., 2019). Yet, despite extensive work, the relative roles of ice-sheet dynamics and carbon-cycle feedbacks, and their timing remain poorly constrained.

Proposed explanations for the MPT can be broadly grouped into three categories: (i) internal ice-sheet dynamics, most notably the regolith hypothesis invoking progressive changes in basal conditions leading to the exposure of high-friction crystalline bedrock (Clark et al., 2006; Clark and Pollard, 1998); (ii) changes in ice-sheet geometry and extent, particularly involving North American and/or Antarctic ice sheets (An et al., 2024; Bintanja and Van De Wal, 2008; Elderfield et al., 2012; Raymo et al., 2006; Wirths et al., 2025); and (iii) feedbacks associated with long-term changes in the global carbon cycle, including deep-sea carbon storage and atmospheric pCO_2 variability (Berger et al., 1999; Chalk et al., 2017; Farmer et al., 2019; Lear et al., 2016; Qin et al., 2022; Shackleton, 2000; Thomas et al., 2022; Willeit et al., 2019). Increasing attention has been paid to the potential role of marine carbon cycle processes (Herbert, 2023), which are closely linked to changes in deep ocean circulation during the MPT (Hall et al., 2001; Hasenfratz et al., 2019; Kim et al., 2021; Li et al., 2026; Martínez-Garcia et al., 2010; Pena and Goldstein, 2014; Qin et al., 2022; Raymo et al., 1997). A "thermohaline circulation crisis" (Pena and Goldstein, 2014) (THC) was proposed for the deep Atlantic across the MPT, but the magnitude and extent of such an event has been questioned recently (Basak et al., 2026; Hines et al., 2024; Williams et al., 2024). Furthermore, recent findings from Allan Hills blue ice area of Antarctica show no significant decline in mean atmospheric pCO_2 over the MPT (Marks-Peterson et al., 2026), which does not necessarily preclude changes in the glacial values of atmospheric pCO_2 because the mean values are likely weighted towards interglacial periods. Forthcoming atmospheric pCO_2 measurements from the Beyond-EPICA ice core are highly anticipated, and will likely resolve the timing and magnitude of atmospheric pCO_2 changes across the MPT.

Whilst numerous studies implicate enhanced carbon storage in the deep sea and lowered glacial atmospheric pCO_2 across the MPT (Billups et al., 2018; Chalk et al., 2017; Farmer et al., 2019; Gildor and Tziperman, 2001; Hodell et al., 2003; Jaccard et al., 2013; Lear et al., 2016; Sigman et al., 2010; Starr et al., 2021; Thomas et al., 2022), no direct comparisons of the temperature and salinity controls on the density of deep water masses have been made between the North Atlantic and Pacific Ocean basins across the transition. This limits assessment of large-scale changes in abyssal density structure, and their potential role in carbon storage and atmospheric pCO_2 change (Adkins, 2013; Broecker and Peng, 1998, 1983). Here, we combine new and previously published records of Mg/Ca-derived deep-water temperature and oxygen isotopic composition of seawater ($\delta^{18}O_{seawater}$), a proxy for both ice volume and salinity, to evaluate how abyssal ocean density structure changed across the MPT.

Benthic $\delta^{18}O$ records are invaluable tools for reconstructing glacial-interglacial variability of the Quaternary (Shackleton, 1967; Shackleton and Opdyke, 1973). However, interpretation of benthic $\delta^{18}O$ records is complicated because the signal is dependent on both temperature and the $\delta^{18}O_{seawater}$, the latter varying with global ice volume and regional hydrography including salinity changes at sites of deep-water formation (Waelbroeck et al., 2002). Deconvolution of benthic $\delta^{18}O$ into its temperature and $\delta^{18}O_{seawater}$ components has been accomplished by paired measurement of Mg/Ca and $\delta^{18}O$ of calcite (Elderfield et al., 2010, 2012; Ford et al., 2016; Ford and Raymo, 2020; Hasenfratz et al., 2017, 2019; Sosdian and Rosenthal, 2009), with estimates of propagated uncertainty (Thirumalai et al., 2016). Other indirect approaches include inverse modelling that combines benthic $\delta^{18}O$ data with ice sheet models of varying complexity (Berends et al., 2021b; Bintanja and Van De Wal, 2008) and an iterative process-based approach that assesses changes in relationships between the oxygen isotopic composition of ice ($\delta^{18}O_{ice}$), sea level, temperature, and $\delta^{18}O_{seawater}$ (Rohling et al., 2021). More recently, changes in global mean sea surface temperatures (ΔGMSST) combined with proxy-based deep ocean temperature estimates, have been used to infer changes in mean ocean temperature (ΔMOT), enabling separation of temperature and ice volume components from a global benthic $\delta^{18}O$ stack (Clark et al., 2025). These different approaches can yield widely divergent interpretations of Quaternary temperature and ice volume evolution. For example, during Marine Isotope Stage (MIS) 22 (~900 ka), Rohling et al. (2021) infer a substantial increase in ice volume with limited deep-water cooling, consistent with earlier Mg/Ca-based reconstructions (Elderfield et al., 2012; Ford and Raymo, 2020). In contrast, the reconstruction of Clark et al. (2025) shows pronounced deep-water cooling with relatively little change in ice volume across the MPT.

Here we present a new 1.5-million-year-long record of North Atlantic deep-water temperature, using Mg/Ca measured in calcite of two infaunal benthic foraminifera (*Uvigerina peregrina* and *Globobulimina affinis*) from sediment cores recovered at International Ocean Discovery Program (IODP) Site U1385 (37°34.3′N, 10°7.6′W, 2578 metres below sea level [mbsl]) from the Iberian Margin (Hodell et al., 2015, 2023) (Figs. 1, S1 and S2; Table 1). The Mg/Ca-derived temperature is paired with benthic $\delta^{18}O$ to isolate the $\delta^{18}O_{seawater}$ signal (Sect. 2.3; Figs. 2 and S3). Our record provides an important complement to existing North Atlantic data from Deep Sea Drilling Project (DSDP) Site 607 (Sosdian and Rosenthal, 2009), where Mg/Ca-derived temperature estimates were based partly on *Cibicidoides wuellerstorfi*. These results were called into question because this epibenthic taxa can be affected by changes in carbonate ion concentrations of bottom waters (Yu and Broecker, Wallace, 2010) (Sect. 3.1; Supplement). This criticism was subsequently refuted (Sosdian and Rosenthal, 2010) prompting additional Mg/Ca measurements of infaunal benthic taxa (*Uvigerina* spp.) at Site 607 (Ford et al., 2016).

We combine (stack) North Atlantic records from Sites U1385 and 607 (Ford et al., 2016; Sosdian and Rosenthal, 2009) and compare them with equivalent Pacific records (Sites 1123 and 1208 (Elderfield et al., 2012; Ford and Raymo, 2020)) to reconstruct the basinal histories of temperature and salinity change (Sect. 2.5–2.6). The Atlantic and Pacific records are then combined with Site 1094 from the South Atlantic sector of the Southern Ocean (Hasenfratz et al., 2019) (Figs. 1, S1 and S2; Table 1) to produce globally distributed stacks. Although the number of deconvolved benthic Mg/Ca–$\delta^{18}O$ records available for stacking is few over the past 1.5 million years (Myr), some distinct differences emerge in the patterns of inferred deep ocean temperature and salinity change between the North Atlantic and Pacific basins.

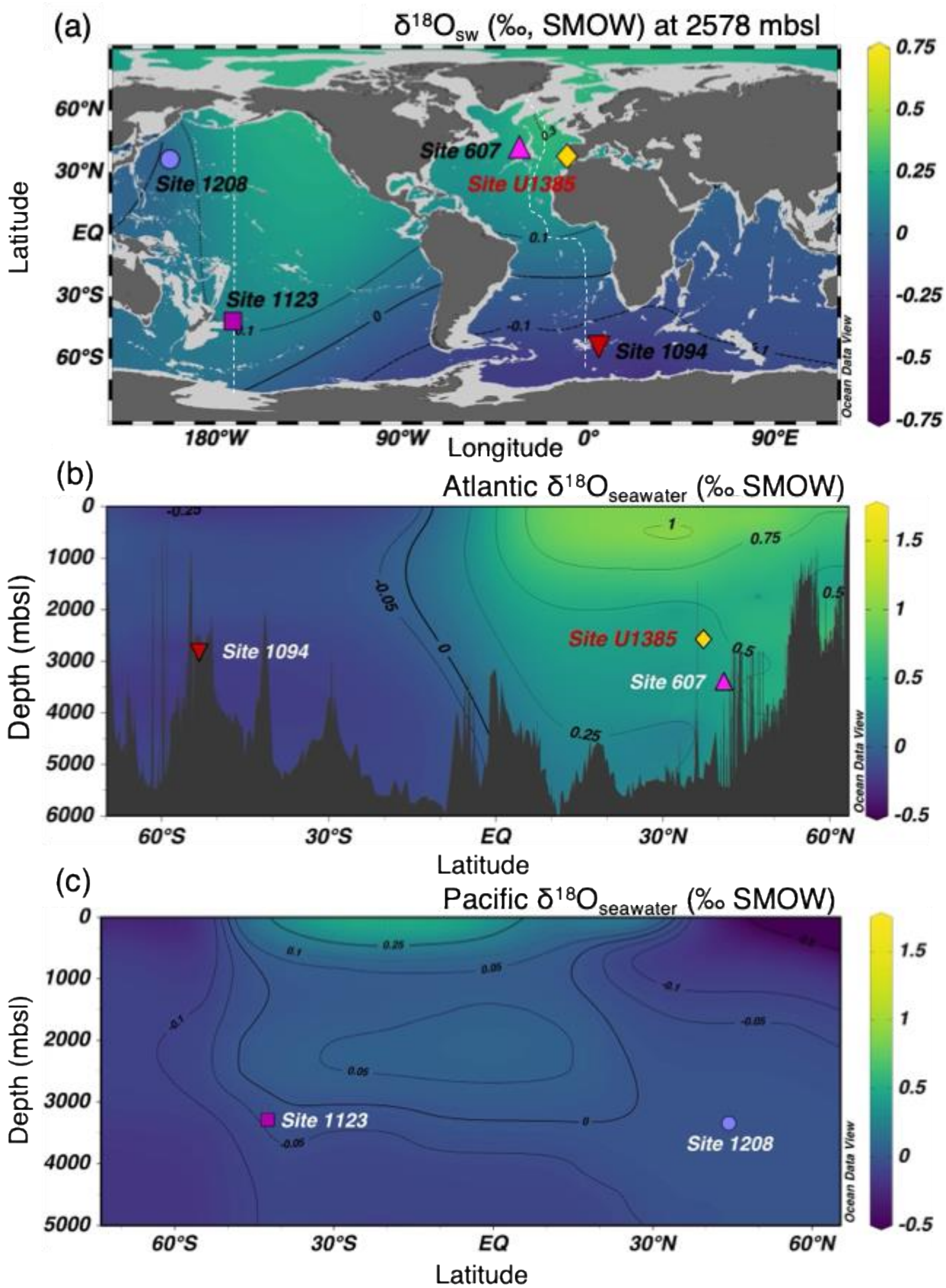

(a)
δ18Osw (‰, SMOW) at 2578 mbsl
Site 607
Site U1385
Site 1208
Site 1123
Site 1094
Latitude
Longitude
180°W
90°W
0°
90°E
60°N
30°N
EQ
30°S
60°S
Ocean Data View
(b)
Atlantic δ18Oseawater (‰ SMOW)
Depth (mbsl)
Site 1094
Site U1385
Site 607
Latitude
60°S
30°S
EQ
30°N
60°N
Ocean Data View
(c)
Pacific δ18Oseawater (‰ SMOW)
Depth (mbsl)
Site 1123
Site 1208
Latitude
60°S
30°S
EQ
30°N
60°N
Ocean Data View

Figure 1: Meridional profiles of deep-water $\delta^{18}O_{seawater}$ showing the site locations. (a) $\delta^{18}O_{seawater}$ at 2578 metres below sea level (mbsl), corresponding to the depth of IODP Site U1385 (this study; yellow diamond) in the Northeast Atlantic, along with the geographic location of other sites referenced in the text: North Atlantic DSDP Site 607 (Ford et al., 2016; Sosdian and Rosenthal, 2009) (pink triangle) Southwestern Pacific ODP Site 1123 (Elderfield et al., 2012) (purple square); North Pacific ODP Site 1208 (Ford and Raymo, 2020) (lilac circle); and the Southern Ocean ODP Site 1094 (Hasenfratz et al., 2019) (red inverted triangle) located in the Atlantic sector of the Antarctic Zone. Meridional transects shown in panels (b) and (c) are indicated by white dashed lines. (b and c) Atlantic and Pacific meridional profiles of deep-water $\delta^{18}O_{seawater}$ (‰, SMOW) showing site locations. Maps were created using GLODAPv2.2021 and GLODAPv2.2023 and GEOSECS in Ocean Data View (Schlitzer, 2019; http://odv.awi.de). Data for panel (c) are from (LeGrande and Schmidt, 2006).

Table 1: Site location details and modern-day deep-water properties.

Site and Citation	Latitude	Longitude	Depth (m)	$\delta^{18}O_{seawater}$ (‰)	Temperature (°C)	Salinity (PSS-78, unitless)*
Iberian Margin: U1385 (This study; Birner et al., 2016)	37°34.3′N	10°7.6′W	2578	~0.2	~3.3 (Hodell et al., 2014)	~35 (Hodell et al., 2014)
MD01-2444 (Skinner et al., 2007)	37°33′N	10°08′W	2637	~0.2		
MD99-2334 (Skinner et al., 2003)	37°48′N	10°10′W	3146	~0.2 (Skinner et al., 2003)	~2.8 (Skinner et al.,2003)	~34.9 (Hodell et al., 2014)
DSDP 607 (Sosdian and Rosenthal, 2009; Ford et al., 2016)	41°00′N	32°58′W	3427	~0.2	~2.6 (Sosdian & Rosenthal, 2009)	~35 (Sosdian & Rosenthal, 2009)
Piston Core Chain 82-24-23PC (Sosdian and Rosenthal, 2009)	43°00′N	31°00′W	3406			
ODP 1123 (Elderfield et al., 2012)	41°47.2′S	171°29.9′W	3290	-0.05 (Elderfield et al., 2010)	~1.3 (Elderfield et al., 2010; Adkins et al., 2002)	34.73 (Adkins et al., 2002)
ODP 1208 (Ford and Raymo, 2020)	36°7.2′N	158°12.0′E	3346	~-0.03	~1.5	34.67
ODP 1094 (Hasenfratz et al., 2019)	53°10′S	5°07′E	2807	~-0.05	~0.5	34.47

*Note: All salinity values reported follow the Practical Salinity Scale (PSS-78) and are unitless.

Unless otherwise stated, temperature and salinity values are from GLODAPv2.2021 and GLODAPv2.2023 and GEOSECS accessed via Ocean Data View (Schlitzer, 2019; http://odv.awi.de), while $\delta^{18}O_{seawater}$ data for Sites 1123 and 1208 are from LeGrande and Schmidt (2006). Coordinates and water depths are taken from the original site publications cited in the first column.

All study sites are deeper than 2500 m and are therefore assumed to be representative of the deep ocean (Figs. 1, S1 and S2; Table 1). Today, Sites U1385 (2578 mbsl) and 607 (3427 mbsl; (Ford et al., 2016; Sosdian and Rosenthal, 2009)) are bathed by North Atlantic Deep Water (NADW) and exhibit similar seawater physical properties (Table 1). Pacific Sites 1123 (3290 mbsl; (Elderfield et al., 2012)) and 1208 (3346 mbsl; (Ford and Raymo, 2020)) are located within Lower Circumpolar Deep Water (LCDW) and Pacific Deep Water (PDW) (Elderfield et al., 2012; Ford and Raymo, 2020; Insua et al., 2014), respectively, and share broadly similar physical properties originating from the Southern Ocean (Talley, 2013). The deep western boundary current (DWBC) of the Southwest Pacific is the main pathway through which most of the cold deep water formed around Antarctica enters the Pacific Ocean (Chandler et al., 2024). The deep water gradually mixes as it flows northward modifying its properties, leading to the formation of Pacific Deep Water (PDW). Given the locations of Site 1123 within the DWBC and 1208 in the PDW, it is reasonable to assume they broadly reflect conditions in the deep Pacific.

Deep Pacific sites are ~1.2 °C colder and ~0.3 lower in salinity (PSS-78) than those in the North Atlantic, reflecting the formation of relatively warm and salty NADW (Figs. S1 and S2; Table 1). Correspondingly, the $\delta^{18}O_{seawater}$ values of the Atlantic sites are on average higher (~0.25 ‰) higher than those of the deep Pacific (Fig. 1; Table 1) (Frew et al., 2000). The Atlantic and Pacific records are merged with Site 1094 (2807 mbsl; (Hasenfratz et al., 2019)) from the South Atlantic sector of the Southern Ocean, which is currently bathed by LCDW.

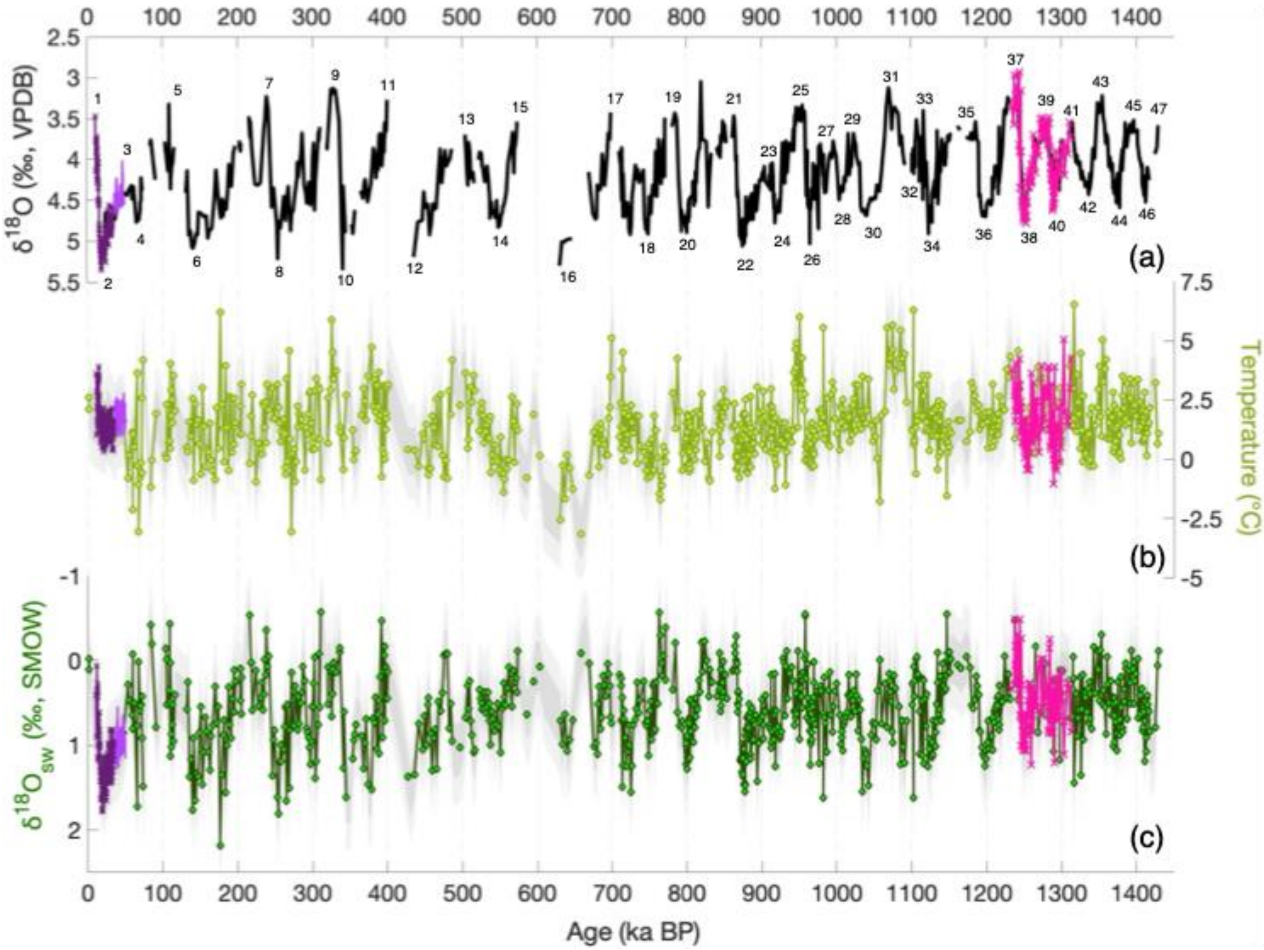

Figure 2: Iberian Margin deep-water Mg/Ca-derived temperature and $\delta^{18}O_{seawater}$ estimated using PSU Solver. (a) Composite benthic $\delta^{18}O$ record, primarily *Uvigerina peregrina,* with *Cibicidoides wuellerstorfi* and *Globobulimina affinis* values adjusted to *Uvigerina peregrina* by +0.64 ‰ and –0.30 ‰ respectively (black line). Numbers denote Marine Isotope Stage (MIS) interglacials (odd, above) and glacials (even, below). (b) Mg/Ca-derived deep-water temperature (light green line and markers) with 1σ and 2σ uncertainty envelopes (dark and light grey, respectively) incorporating both analytical and calibration uncertainties. (c) Deconvolved $\delta^{18}O_{seawater}$ (dark green line and markers; note the inverted axis) with uncertainties as in (b). All panels show Site U1385 (this study) together with records from Birner et al. (2016) (pink lines with crosses during MIS 41–37), MD01-2444 (Skinner and Elderfield, 2007) (light purple line) and MD99-2334 (Skinner et al., 2003) dark purple line with crosses).

2 Materials and Methods

2.1 Site details and chronology

Four holes drilled at Site U1385 were spliced to produce a continuous composite section extending to 166.5 metre composite depth (mcd), corresponding to a basal age of ~1.45 Ma during Marine Isotope Stage (MIS) 47 (Hodell et al., 2015, 2023). The

Site U1385 age model was established by alignment of the benthic oxygen isotope ($\delta^{18}O$) record to the LR04 reference stack (Hodell et al., 2023; Lisiecki and Raymo, 2005), with chronostratigraphic ages assigned by linear interpolation between age-depth control points.

All previously published records used to compile the ocean stacks are presented on their original published age models. Most are based on alignment of benthic foraminiferal $\delta^{18}O$ to LR04, including DSDP Site 607 combined with Chain 82-24-23PC (Ford et al., 2016; Sosdian and Rosenthal, 2009), and Ocean Drilling Program (ODP) Site 1123 (Elderfield et al., 2012). ODP Site 1208 (Ford and Raymo, 2020) was aligned to the Prob-stack using the HMM-Stack MATLAB code (Ahn et al., 2017; Ford and Raymo, 2020; Lin et al., 2014: Butcher et al., 2017), which is also based on the LR04 age model. The ODP Site 1094 age model (Hasenfratz et al., 2019) was derived by graphical alignment of benthic $\delta^{18}O$ to LR04, with the original chronology of (Jaccard et al., 2013) retained where benthic foraminifera were sparse (e.g. MIS 4).

The Iberian Margin piston cores MD99-2334 and MD01-2444 were independently aligned to Greenland ice-core records through synchronisation of Dansgaard–Oeschger events recorded in planktonic $\delta^{18}O$ (Shackleton, 2000; Skinner et al., 2003; Skinner and Elderfield, 2007). Owing to the close agreement in both structure and absolute benthic $\delta^{18}O$ values with Site U1385 over the interval of overlap, no further adjustments to these published age models were applied.

2.2 Stable isotopes

Oxygen and carbon isotopes were measured previously using *Cibicidoidies wuellerstorfi* from the >212 µm sediment coarse fraction (Hodell et al., 2023, 2026). Additional analyses were made using *Uvigerina peregrina* and *Globobulimina affinis* selected from the 212–355 µm coarse fraction. All benthic oxygen isotope data were corrected to *Uvigerina* using an offset of 0.64‰ for *C. wuellerstorfi* and -0.3‰ for *G. affinis*. Tests were crushed between glass slides to facilitate cleaning. Isotopic measurements were made at the Godwin Laboratory for Palaeoclimate Research, Department of Earth Sciences, University of Cambridge following previously described methods (Hodell et al., 2015). Instrument precision was better than ±0.08 ‰ (1σ) for $\delta^{18}O$ and ±0.06 ‰ (1σ) for $\delta^{13}C$.

2.3 Foraminiferal Mg/Ca analyses

Benthic Mg/Ca, deep-water temperature and $\delta^{18}O_{seawater}$ records from Site U1385 extend back to ~1.45 Ma, spanning MIS 1–47. Mg/Ca measurements on *Uvigerina peregrina* and *Globobulimina affinis* were conducted at ~20 cm intervals, corresponding to a mean temporal resolution of ~2000 years (yr), except for two intervals sampled at higher resolution: ~4 cm spacing between ~980–860 thousand years ago (ka) over MIS 27–21, and ~5 cm spacing between ~1300–1240 ka (MIS 40–37) (Birner et al., 2016) yielding a temporal resolution of ~500 yr.

Three noticeable breaks (>15 kyr) occur in the Mg/Ca-derived temperature and $\delta^{18}O_{seawater}$ records because of low foraminiferal abundance between MIS 6–5 (~132–116 ka), and MIS 16–15 (~630–603 ka). In addition, a near 30-kyr hiatus removed the interval at Site 339-U1385 between MIS 12–11 (~430-400 ka) at Termination V (Hodell *et al.*, 2015, 2023), which has now been recovered in companion Site 397-U1385 (Hodell et al., 2026). To produce a near-continuous Iberian Margin record spanning the past 1.5 Myr, Site U1385 records were supplemented through the last glacial cycle with Mg/Ca-derived temperature and $\delta^{18}O_{seawater}$ data measured on *Globobulimina affinis* at nearby piston cores MD01-2444 covering 50–35 ka during the early glacial interval (Skinner and Elderfield, 2007), and MD99-2334 spanning 35–10 ka during the late glaciation (Skinner et al., 2003) (Fig. 2; Table.1). Following Skinner et al. (2007) a constant temperature offset of +0.6 °C was applied to Mg/Ca-derived temperatures from the deeper Core MD99-2334 to account for cooler modern deep-water temperature at that site location ((Hodell, 2014; Skinner et al., 2003, 2007; Skinner and Elderfield, 2007); Table 1).

After data quality screening (Sect. 2.4), we report Mg/Ca results for 864 samples of *Uvigerina peregrina* and 202 samples of *Globobulimina affinis*. All samples were oxidatively cleaned following the procedure of Barker, Greaves and Elderfield (2003). Trace elements were measured at the Godwin Laboratory for Palaeoclimate Research (Cambridge, UK) using inductively coupled plasma-optical emission spectroscopy (ICP-OES). Most analyses were performed on a Varian VISTA instrument (Birner et al., 2016) with the remaining ~180 samples measured using an Agilent 5100 ICP-OES. Both instruments used the intensity-ratio calibration method of de Villiers, Greaves and Elderfield (2002). Interlaboratory comparison studies have validated the use of laboratory standards employed as reference materials for foraminiferal Mg/Ca analyses (Greaves et al., 2008). Repeated measurements of standards showed instrument precision for Mg/Ca determinations to be better than 0.5 % relative standard deviation (r.s.d.) (Greaves, 2008; Greaves et al., 2008; de Villiers et al., 2002). Based on long-term standard reproducibility and 47 sets of replicate analyses (including four triplicates) measured on multiple aliquots of the same sample, the pooled standard deviation is ±0.09 mmol mol^{-1} (1σ), corresponding to a mean precision of 8.2 % r.s.d. (See Data Repository Table S4).

Mg/Ca–derived deep-water temperatures from *Uvigerina peregrina* and *Globobulimina affinis* show generally good agreement in both variability and mean values within uncertainty (1.4 ± 1.5 °C and 1.6 ± 1.0 °C, respectively) (Fig. S3a). Both species record similar mean $\delta^{18}O_{seawater}$ values (~ 0.6 ± 0.4 ‰; Fig. S3b). This agreement is consistent with the application of species-specific Mg/Ca–temperature calibrations applied in this study (Elderfield et al., 2006, 2010, 2012a; Weldeab et al., 2016) and justifies combining the two datasets. The individual *Uvigerina peregrina* and *Globobulimina affinis* time series were used as inputs for the PSU Solver calibration procedures described in Sect. 2.5 and combined into single records of deep-water temperature and $\delta^{18}O_{seawater}$ (Fig. 2).

2.4 Data quality evaluation

Mg/Ca ratios derived from foraminiferal calcite tests can be used to estimate palaeotemperatures provided that stringent cleaning procedures are followed (Barker et al., 2003; Larsson and Jung, 2025). To evaluate the efficiency of these cleaning procedures and to assess the effects of authigenic precipitation, we analysed element/Ca ratios of co-measured trace elements—primarily Fe and Mn, but also Al, Ba, K, Na, Si, Ti and Zn (Barker et al., 2003; Elderfield et al., 2012; Greaves, 2008;

Hasenfratz et al., 2017). Contamination by silicates and clay minerals can lead to significant uncertainty in measured Mg/Ca values. Therefore, the removal of contaminant silicates is a critical step in the cleaning protocol, and its success can be evaluated through downcore covariation of Mg/Ca and Fe/Ca (or Al/Ca) records (Barker et al., 2003). Mg/Ca records from the two foraminiferal species were assessed separately, as *Globobulimina affinis* is known to exhibit elevated Mg/Ca ratios relative to other benthic foraminiferal species (Skinner et al., 2003; Weldeab et al., 2016). At Site U1385, five *Uvigerina peregrina* and three *Globobulimina affinis* samples were excluded from the Mg/Ca dataset following identification of anomalously high co-occurring Fe/Ca and Mg/Ca values (Barker et al., 2003). Sample exclusion was based on co-occurring Fe/Ca–Mg/Ca anomalies rather than a fixed Fe/Mg threshold (Fig. S4). The Mg/Ca dataset presented here includes *Uvigerina peregrina* samples with Fe/Ca and Fe/Mg values of up to 0.45 mmol mol^{-1} and 0.33 mol mol^{-1}, respectively (and *Globobulimina affinis* values up to 0.79 mmol mol^{-1} and 0.28 mol mol^{-1}), which exceed the typical Fe/Ca (<0.1 mmol mol^{-1}) and Fe/Mg (<0.03 mol mol^{-1}) values reported by Barker, Greaves and Elderfield (2003) and Elderfield et al. (2012).

Consistent with observations of *Uvigerina* spp. at Site 1123 (Elderfield et al., 2012), Mn/Ca values for *Uvigerina peregrina* at Site U1385 show a slight downcore increase, with lowest glacial values rising from ~0.012 mmol mol^{-1} at 60 ka to ~0.045 mmol mol^{-1} at ~1415 ka (Fig. S5). Although the maximum Mn/Ca value for *Uvigerina peregrina* at Site U1385 (0.28 mmol mol^{-1}) is lower than the 0.36 mmol mol^{-1} reported for Site 1123 (Elderfield et al., 2012), Mn/Ca values exceeding ~0.1 mmol mol^{-1} may suggest the presence of authigenic Mn–Fe-oxide coatings on some foraminiferal tests (Elderfield et al., 2012; Hasenfratz et al., 2017, 2019). The incorporation of Mn into calcite tests has been shown to be species-specific (van Dijk et al., 2025). In *Uvigerina peregrina*, Mn/Ca values range from 0.01 to 0.28 mmol mol^{-1}, while in *Globobulimina affinis*, values are generally higher, ranging from 0.04 to 1.88 mmol mol^{-1}, with two anomalous specimens exceeding this upper value. Despite these elevated Mn/Ca values, the absence of a positive correlation between Mn/Ca and Mg/Ca indicates that the presence of Mn–Fe oxides does not significantly influence Mg/Ca variability. We therefore interpret the higher Mn/Ca values as reflecting variable contributions from authigenic Mn–Fe-oxide coatings (Skinner et al., 2003), or from species-specific Mn incorporation during biomineralization (van Dijk et al., 2025).

Diagenetic Mn-Fe-oxide coatings commonly form on foraminiferal shells in deep-sea sediment cores used in palaeoceanographic reconstructions. In oxygenated porewater dissolved manganese is precipitated onto carbonate tests as Mn^{4+} oxides, later becoming remobilized as Mn^{2+} and forming Mn-rich oxide coatings when organic matter undergoes anaerobic decomposition deeper in the sediment (Barker et al., 2003; Boiteau et al., 2012). These Mn-rich coatings can substantially impact bulk Mg/Ca ratios and introduce bias into deep-water temperature reconstructions (Hasenfratz et al., 2017). Site specific studies reveal relatively consistent Mg/Mn ratios in foraminiferal coatings, ranging globally between 0.17–0.32 mol mol^{-1} [see Hasenfratz et al. (2017) Table 1 and references therein]. Regionally the upper end of this range—between 0.26 to 0.32 mol mol^{-1}—is most applicable to the Atlantic Ocean, although individual sites may deviate notably from basin-wide averages (Hasenfratz et al., 2017). These Mg/Mn ratios can be used to correct Mg/Ca ratios associated with the calcite lattice using the following equation (Hasenfratz et al., 2017):

$$\mathrm{Mg/Ca_{corrected}} = \mathrm{Mg/Ca_{measured}} - \left(\mathrm{Mn/Ca_{measured}} \times \mathrm{Mg/Mn_{coating}}\right) \quad (1)$$

To maintain consistency, we applied a $Mg/Mn_{coating}$ correction following Equation 1, with the $Mg/Mn_{coating}$ term fixed at 0.32 mol mol^{-1}, and applied uniformly to all Mg/Ca data (Hasenfratz et al., 2017; de Lange et al., 1992) (Fig. S6). This value represents the maximum adjustment in the direction of lower temperatures and yields the least discrepancy between Site U1385 temperatures and those from the Pacific and South Atlantic. The correction has minimal influence on glacial Mg/Ca values. In total, Mg/Ca was initially determined on 911 *Uvigerina peregrina* and 264 *Globobulimina affinis* samples. After quality control, we retain Mg/Ca results for 864 samples of *Uvigerina peregrina* (including replicates) and 202 samples of *Globobulimina affinis* measurements, having excluded 42 and 59 samples, respectively, based on co-measured trace element indicators of potential contamination. Samples were rejected according to the following criteria:

- Clay contamination: Low [Ca] (<10 ppm) coupled with high Na/Ca (>5.5 mmol mol^{-1}), and K/Ca (>0.4 mmol mol^{-1}), almost always associated with elevated Mg/Ca.
- Additional indicators of clay influence: Al/Ca > 0.4 mmol mol^{-1}, Si/Ca > 0.4 mmol mol^{-1}, Ti/Ca > 0.005 mmol mol^{-1}, or very low Mn/Fe (< 0.1 mol mol^{-1}) due to elevated Fe/Ca.
- Analytical blank effects: Low [Ca] combined with anomalously high Mg/Ca values, suggesting contamination during measurement.

2.5 PSU Solver: Calibration equations for Mg/Ca-derived deep-water temperature and $\delta^{18}O_{seawater}$

Deep-water temperature and $\delta^{18}O_{seawater}$ estimates were calculated for Site U1385 over the past 1.5 Ma using an updated Python version of Paleo-Seawater Uncertainty Solver (PSU Solver) originally developed in MATLAB (Thirumalai et al., 2016). Uncertainties associated with Mg/Ca–temperature calibration slopes and intercepts were propagated explicitly within a Monte Carlo framework by sampling calibration slopes and intercepts within their reported uncertainties during each iteration (n = 1000). Input data comprise foraminiferal Mg/Ca and benthic $\delta^{18}O$ measurements. Standard laboratory uncertainties of 0.08 ‰ for $\delta^{18}O$ and 0.05 mmol mol^{-1} for Mg/Ca were applied as inputs to the PSU Solver (Thirumalai et al., 2016). Species-specific Mg/Ca–temperature calibrations were employed within the PSU Solver framework (Table 2).
For *Uvigerina peregrina,* we used the linear Mg/Ca–temperature calibration of Elderfield et al. (2012):

$$\mathrm{Mg/Ca}\ [\mathrm{mmol\ mol^{-1}}] = 1.0 + (0.1 \pm 0.013 \times \mathrm{T}\ [°\mathrm{C}]) \quad (2)$$

Core-top Mg/Ca-derived temperatures (~2.5 °C; Figs. 2 and S3) are consistent with modern deep-water temperatures (~2–3 °C) at the Iberian Margin (Hodell et al., 2014; Skinner et al., 2003), supporting the applicability of the Elderfield et al. (2012) Mg/Ca–temperature calibration at this site.
For *Globobulimina affinis*, we applied the calibration of Weldeab, Arce and Kasten (2016):

$$\mathrm{Mg/Ca}\ [\mathrm{mmol\ mol^{-1}}] = 2.22 \pm 0.19 + (0.36 \pm 0.02 \times \mathrm{T}\ [°\mathrm{C}]) \tag{3}$$

To reconstruct $\delta^{18}O_{seawater}$ we used the oxygen-isotope palaeothermometry equation (Elderfield et al., 2010, 2012):

$$\mathrm{T}\ [°\mathrm{C}] = 16.9 - 4.0 \times (\delta^{18}\mathrm{O}_{calcite}\ [‰] - \delta^{18}\mathrm{O}_{seawater}\ [‰] + 0.27) \tag{4}$$

Age model uncertainty was set at ±2 kyr, which represents both the optimal resolution for combining the records of differing resolution and the mean resolution of the five records.

Table 2: Species-specific Mg/Ca–temperature calibrations.

Site	Species	Species specific Mg/Ca (mmol mol $^{-1}$) to temperature (°C) PSU eq 1	Lab; Citation
IODP U1385	*Uvigerina peregrina*	$\mathrm{Mg/Ca} = 1 + (0.1 \pm 0.013 \times \mathrm{T})$ Elderfield et al., 2012	Cambridge: This study (Birner et al., 2016)
IODP U1385	*Globobulimina affinis*	$\mathrm{Mg/Ca} = 2.22 \pm 0.19 + (0.36 \pm 0.02 \times \mathrm{T})$ Weldeab et al., 2016	Cambridge: This study
MD99-2334	*Globobulimina affinis*	$\mathrm{Mg/Ca} = 2.22 \pm 0.19 + (0.36 \pm 0.02 \times \mathrm{T})$ Weldeab et al., 2016	Cambridge: (Skinner et al., 2003)
MD01-2444	*Globobulimina affinis*	$\mathrm{Mg/Ca} = 2.22 \pm 0.19 + (0.36 \pm 0.02 \times \mathrm{T})$ Weldeab et al., 2016	Cambridge: (Skinner et al., 2007)
ODP 1123	*Uvigerina* spp.	$\mathrm{Mg/Ca} = 1 + (0.1 \pm 0.013 \times \mathrm{T})$ Elderfield et al., 2012	Cambridge: (Elderfield et al., 2012)
DSDP 607 + Piston Core Chain 82-24-23PC	*Uvigerina* spp.	$\mathrm{Mg/Ca} = 0.9 + (0.1 \pm 0.013 \times \mathrm{T})$ Elderfield et al., 2012 (modified for reductive cleaning)	LDEO & Rutgers: (Ford et al., 2016)
	Cibicidoides wuellerstorfi	$\mathrm{Mg/Ca} = 1.043 \pm 0.03 \times e\hat{}(0.118 \pm 0.1 \times \mathrm{T})$ Barrientos et al., 2018	LDEO & Rutgers: (Sosdian and Rosenthal, 2009)
	Oridorsalis umbonatus	$\mathrm{Mg/Ca} = 1.317 \pm 0.03 \times e\hat{}(0.102 \pm 0.01 \times \mathrm{T})$ Barrientos et al., 2018	LDEO & Rutgers: (Sosdian and Rosenthal, 2009)
ODP 1208	*Uvigerina* spp.	$\mathrm{Mg/Ca} = 0.9 + (0.1 \pm 0.013 \times \mathrm{T})$ Elderfield et al., 2012 (modified for reductive cleaning)	LDEO & Rutgers: (Ford and Raymo, 2020)
ODP 1094	*Melonis pompilioides*	$\mathrm{Mg/Ca} = 0.742 + (0.119 \pm 0.003 \times \mathrm{T})$ Hasenfratz et al., 2017	ETHZ & Cambridge: (Hasenfratz et al., 2019)

*Abbreviations: LDEO, Lamont-Doherty Earth Observatory (Columbia University, New York, USA); ETHZ, Geological Institute, ETH Zurich (Zurich, Switzerland).

2.6 Stacking temperature and $\delta^{18}O_{seawater}$ records

The rationale for stacking records of temperature and $\delta^{18}O_{seawater}$ is the same as that given for oxygen isotope records (Imbrie et al., 1984; Lisiecki and Raymo, 2005); that is, to improve the signal/noise ratio and reduce the influence of local variability. Although stacked records provide more representative regional and/or global mean signals of temperature and ice volume they also tend to dampen the amplitude of the signal owing to misalignments and smoothing. Stacked deep-water temperature and $\delta^{18}O_{seawater}$ records were constructed for the North Atlantic using Sites U1385 (this study; Birner et al., 2016), MD01-2444 (Skinner and Elderfield, 2007), MD99-2334 (Skinner et al., 2003) and Site 607 (Ford et al., 2016; Sosdian and Rosenthal, 2009). The deep Pacific stack was derived using Sites 1123 (Elderfield et al., 2012) and 1208 (Ford and Raymo, 2020) (Figs. S7 and S8). Globally distributed mean deep ocean temperature (MDOT) and mean deep ocean $\delta^{18}O_{seawater}$ stacks (Figs. 3a and 4a respectively) incorporate these records together with ODP Site 1094 located in the South Atlantic sector of the Southern Ocean (Hasenfratz et al., 2019) (Fig. S9).

Prior to stacking, temperature and $\delta^{18}O_{seawater}$ estimates were interpolated to a regular 3 kyr time step using MATLAB's `interp` function. Uncertainty envelopes were estimated using bootstrap resampling (n = 1000), assuming normally distributed errors defined by the reported standard deviations (1σ) (Figs. 3 and 4). Gaps in the original age models were identified, and interpolated values were excluded where age gaps exceeded ~6 kyr. At each interpolated time step, stacked estimates were calculated using either arithmetic or volumetrically weighted averaging of available basin-scale records. Uncertainties in non-weighted stacks were estimated by propagating the combined calibration and analytical errors in quadrature and incorporating inter-record variance, such that the uncertainty of the mean reflects both measurement uncertainty and the spread between paired estimates. For weighted stacks, basin weights were defined using fixed deep ocean volume fractions following the volumetric approach of Lisiecki and Stern (2016) (see their Table S2) and renormalised to unity at each time step to reflect the ocean volume represented by the available records. This ensures that stacked estimates reflect the relative deep ocean volume of the contributing basins without introducing bias when one or more basins are absent. Only half of the stacked data points (n = 268) include contributions from all three basins (North Atlantic, Southern Ocean and Pacific), together representing 43.6% of the global ocean volume (Table S1). The impact of data gaps in the Site 1094 record appears to exert little influence on the weighted MDOT and mean $\delta^{18}O_{seawater}$ reconstructions (Fig. S10).

At each time step t, volumetrically weighted stacked estimates were calculated as

$$\bar{x}(t) = \sum_{i=1}^{N(t)} w_i\,(t)\,x_i(t), \tag{5}$$

where $x_i(t)$ is the basin-scale estimate (temperature or $\delta^{18}O_{seawater}$) and $N(t)$ is the number of available basins. Weights were defined as

$$w_i(t) = \frac{V_i}{\sum_{j=1}^{N(t)} V_j}. \quad (6)$$

where, V_i denotes the deep ocean volume fraction represented by basin i, and the denominator represents the total volume of all basins available at time t.

Total uncertainty was estimated by propagating intra-basin variance and incorporating an inter-basin variance term that captures the spread of basin-scale estimates about the weighted mean:

$$\sigma^2(t) = \sum_{i=1}^{N(t)} w_i^2(t)\, \sigma_i^2(t) + \sum_{i=1}^{N(t)} w_i(t)(x_i(t) - \bar{x}(t))^2, \quad (7)$$

where $\sigma_i(t)$ represents the reported 1σ uncertainty of basin i, and the second term represents inter-basin variability. Where only a single basin contributed to the stack, the uncertainty reduces to the reported basin 1σ value. This approach assumes that residual chronological misalignment between records is small relative to the interpolated 3 kyr resolution. Uncertainty envelopes incorporate analytical, calibration and age uncertainties propagated through a Monte Carlo framework, with basin-scale uncertainty additionally reflecting inter-site variability.

Change-point analysis was applied to the interpolated stacks (3 kyr resolution) using MATLAB's `findchangepts` function to identify statistically significant shifts in the mean state of the record. The analysis detects a primary breakpoint at ~930 ka in both mean averaged and basin-volume weighted $\delta^{18}O_{seawater}$ stacks, marking the most prominent transition in the time series.

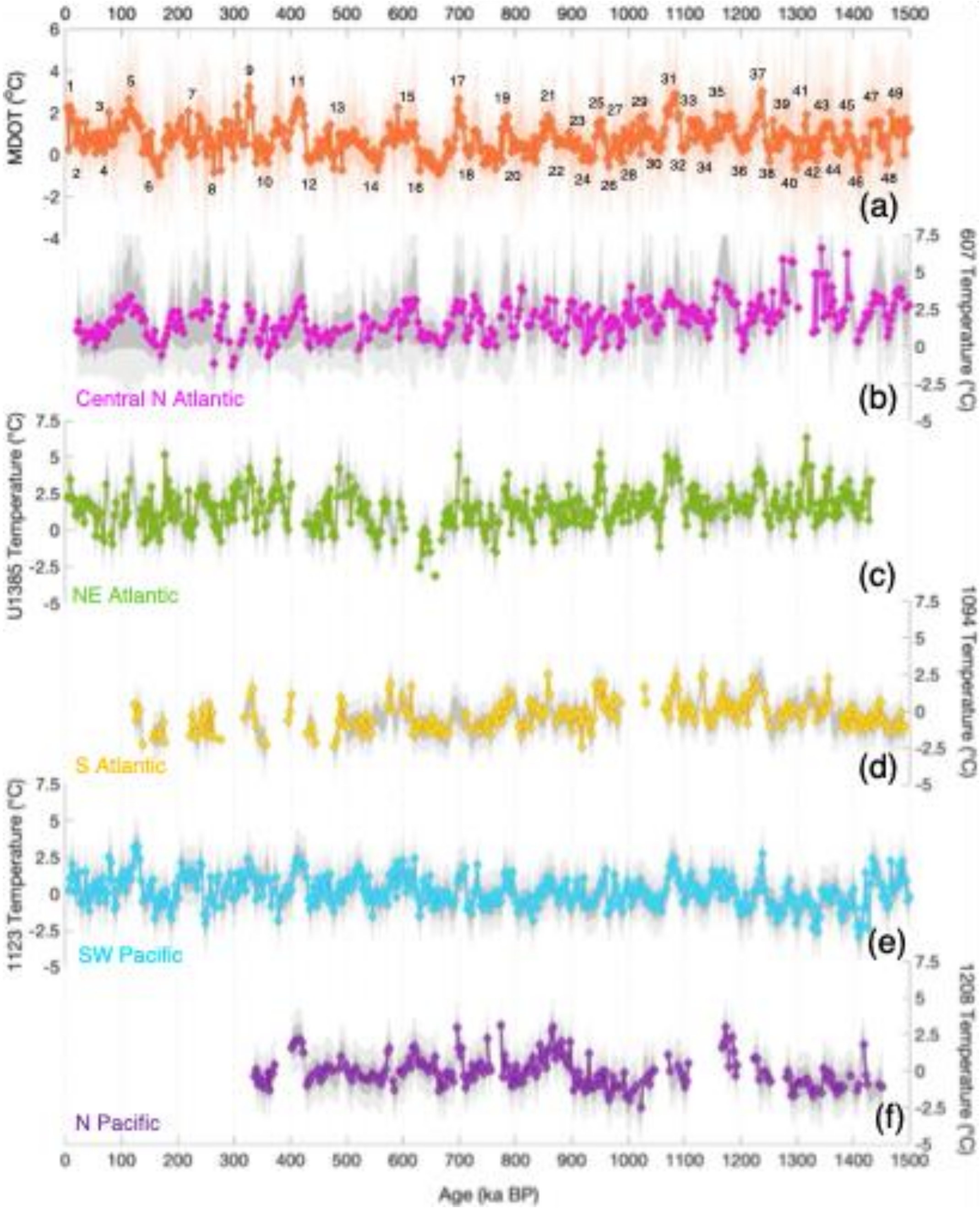

Figure 3: Interpolated and bootstrapped Mg/Ca-derived temperature records for all sites. (a) Mean deep ocean temperature stack (MDOT; this study, orange line and markers), with MIS numbers denoting glacial (below) and interglacial (above) stages. Mg/Ca-derived temperature records for: (b) DSDP Site 607 (Ford et al., 2016; Sosdian and Rosenthal, 2009) (light pink); (c) IODP Site U1385 (this study, including additional Iberian Margin records (Birner et al., 2016; Skinner et al., 2003; Skinner and Elderfield, 2007) (light green); (d) ODP Site 1094 (Hasenfratz et al., 2019) (yellow); (e) ODP Site 1123 (Elderfield et al., 2012) (light blue); and (f) ODP Site 1208 (Ford and Raymo, 2020) (dark purple). Mg/Ca-derived temperature records were interpolated on a 3 kyr interval and subsequently bootstrapped. Shading represents 1 and 2σ error margins (dark and light grey respectively), propagated from both analytical and calibration sources.

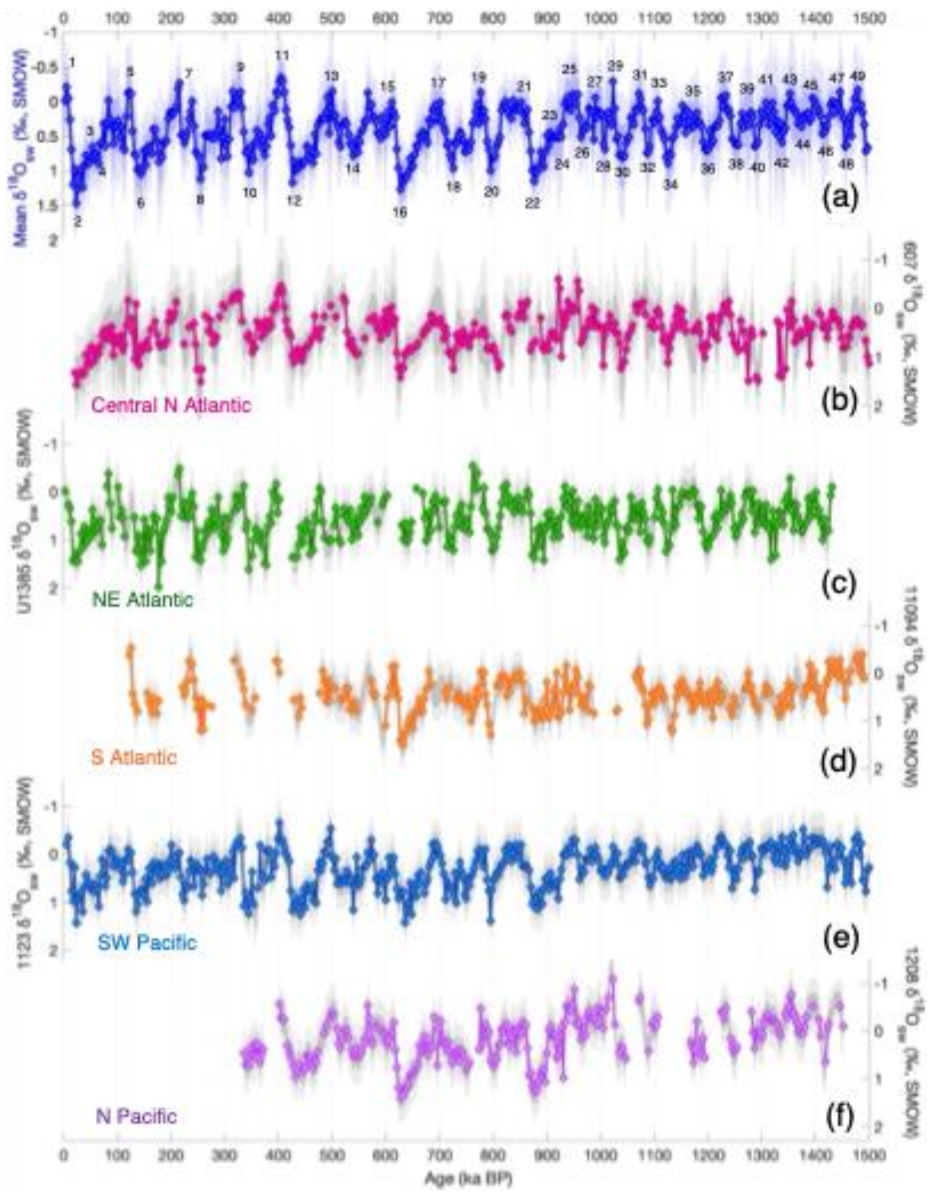

Figure 4: Interpolated and bootstrapped $\delta^{18}O_{seawater}$ records for all sites. (a) Mean $\delta^{18}O_{seawater}$ stack (this study; blue line and markers) with MIS numbers denoting glacial stages (below) and interglacial stages (above). Interpolated and bootstrapped $\delta^{18}O_{seawater}$ records for: (b) DSDP Site 607 (Ford et al., 2016; Sosdian and Rosenthal, 2009) (pink); (c) IODP Site U1385 (this study, including additional Iberian Margin records (Birner et al., 2016; Skinner et al., 2003; Skinner and Elderfield, 2007) (green); (d) ODP Site 1094 (Hasenfratz et al., 2019) (orange); (e) ODP Site 1123 (Elderfield et al., 2012) (blue); and (f) ODP Site 1208 (Ford and Raymo, 2020) (purple). All $\delta^{18}O_{seawater}$ records were interpolated to a 3 kyr interval and subsequently bootstrapped. Shading denotes 1 and 2σ error margins (dark and light grey respectively), propagated from both analytical and calibration uncertainties.

3 Results

3.1 Comparison of Sites U1385 and 607 deep-water records

North Atlantic Sites U1385 and 607 temperature and $\delta^{18}O_{seawater}$ records generally show similar values and trends over the past 1.5 Myr (Figs. 5b and 6b), but there are some differences in the magnitude of the Mg/Ca-derived temperature changes. Greater cooling is expressed at Site 607 where temperatures show decreasing trends of ~1.0 °C between 1500–900 ka and ~1.7 °C over the past 1.5 Myr compared to Site U1385 which shows less cooling. At times, differences between the two temperature records (e.g. between 1180–1150 ka and ~400–350 ka) correspond to Mg/Ca measurements of *Cibicidoides wuellerstorfi* at Site 607, which is more prone to carbonate ion changes and dissolution than infaunal benthic taxa. However, the cooler temperatures at Site 607 cannot be attributed solely to a carbonate ion effect because *Uvigerina* spp. also give high temperatures between ~1400–1300 ka (Ford et al., 2016; Sosdian and Rosenthal, 2009) and may instead reflect hydrographic differences between the eastern and western North Atlantic basins (Chalk et al., 2019). Despite the subtle differences in the records, the close similarity in both temperature and $\delta^{18}O_{seawater}$ data from the two sites supports their integration into a North Atlantic stack. The magnitude of cooling is also supported by a decrease in alkenone SST in the high-latitude of the North Atlantic where deep water is formed (Lawrence et al., 2009).

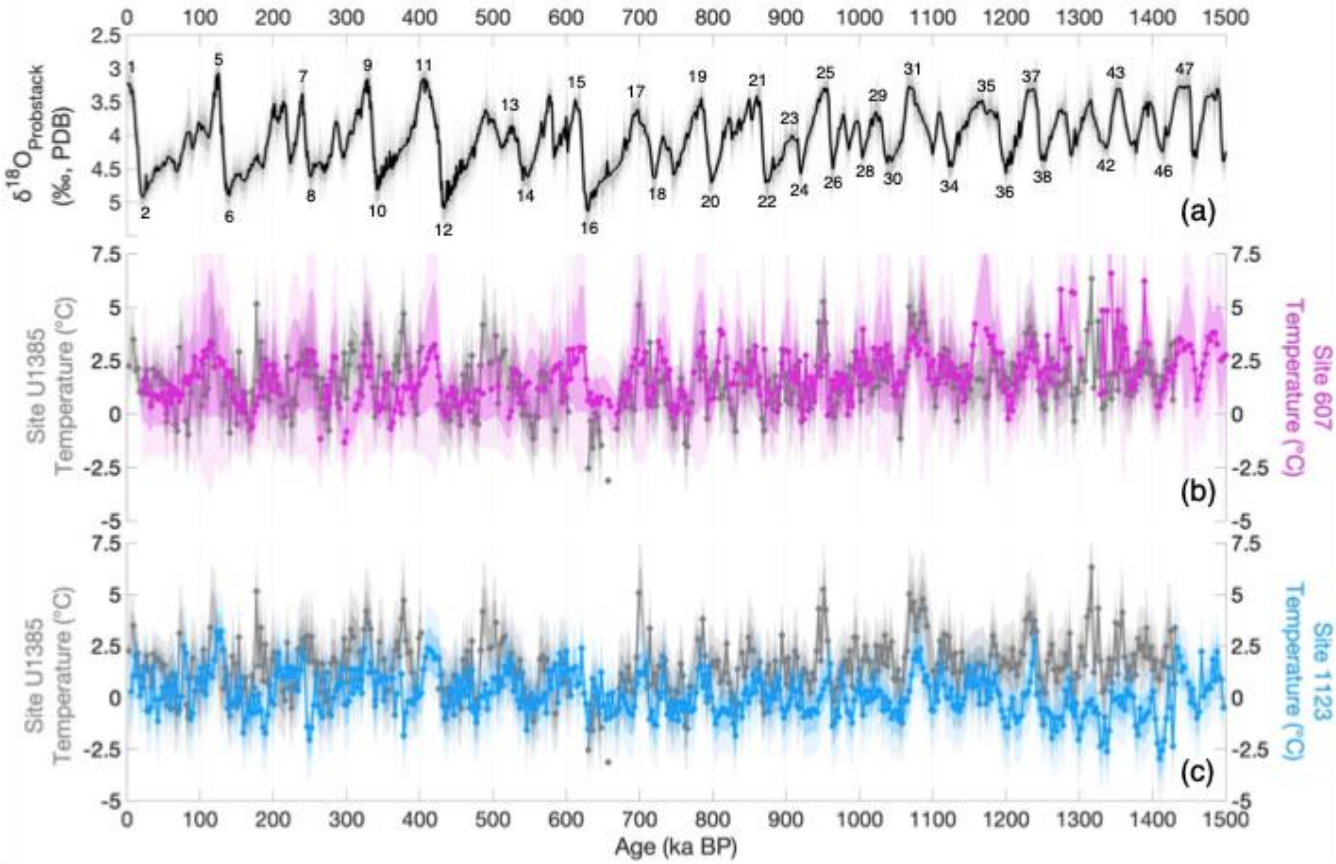

Figure 5: Comparison of Mg/Ca-derived deep-water temperature from Site U1385 versus Sites 607 and 1123. (a) Prob-stack benthic $\delta^{18}O$ (Ahn et al., 2017) (black line), with MIS numbers denoting glacials (below) and interglacials (above). Mg/Ca-derived deep-water temperatures from Site U1385 (grey) are compared with (b) Site 607 (Ford et al., 2016; Sosdian and Rosenthal, 2009) (pink), and (c) Site 1123 (Elderfield et al., 2012) (blue). Site 607 exhibits a gradual cooling through time (Ford et al., 2016; Sosdian and Rosenthal, 2009), whereas Site 1123 documents relatively stable, near-freezing temperatures during glacial maxima (Elderfield et al., 2012). Dark and light shading represent 1 and 2σ uncertainties, respectively, estimated by propagating analytical and calibration uncertainties in quadrature, and accounting for inter-record variance. Records are interpolated to 3 kyr resolution and bootstrapped.

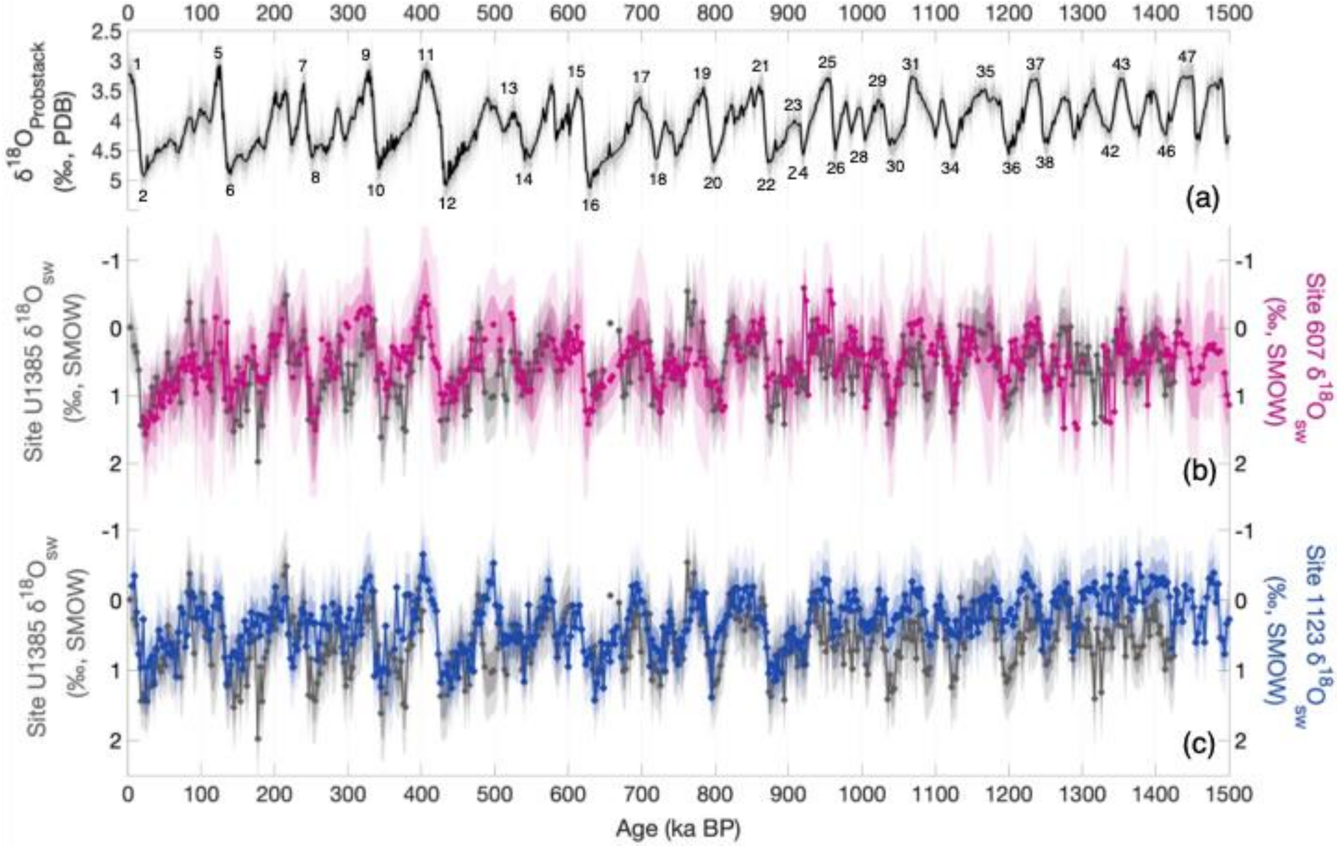

Figure 6: Comparison of benthic $\delta^{18}O_{seawater}$ records from Site U1385 with Sites 607 and 1123. (a) Prob-stack benthic $\delta^{18}O$ (Ahn et al., 2017) (black line), with MIS numbers denoting glacial (even) and interglacial (odd) stages. Deep-water $\delta^{18}O_{seawater}$ from Site U1385 (dark grey) is compared with (b) Site 607 (Ford et al., 2016; Sosdian and Rosenthal, 2009) (dark pink), and (c) Site 1123 (Elderfield et al., 2012) (dark blue). Records are interpolated at a 3 kyr interval and bootstrapped. Dark and light shading indicates 1σ and 2σ uncertainty envelopes, respectively. No clear long-term trend in $\delta^{18}O_{seawater}$ (ice volume/salinity) is observed at Site 607 (Ford et al., 2016; Sosdian and Rosenthal, 2009), whereas Site 1123 records an abrupt increase in Antarctic ice volume (salinity) ~900 ka (Elderfield et al., 2012).

3.2 Deep Atlantic-Pacific gradients in deep-water temperature and $\delta^{18}O_{seawater}$

Whereas the benthic $\delta^{18}O_{calcite}$ records are similar between the Atlantic and Pacific (Fig. 7a), the deconvolved temperature and $\delta^{18}O_{seawater}$ records are not. Comparisons between Atlantic and Pacific deep-water temperature and $\delta^{18}O_{seawater}$ stacks show greater inter-basin differences before ~930 ka than afterwards. From 1500 to 930 ka (MIS 49 to 24), North Atlantic deep-water was on average ~2.5 ± 1.5 °C warmer than the deep Pacific during both glacial and interglacial stages (Fig. 7b). After ~930 ka, this temperature difference decreases to ~1.1 ± 1.4 °C primarily reflecting cooling of glacial North Atlantic deep-water while deep Pacific temperatures show only minor changes. Prior to 930 ka, deep ocean glacial $\delta^{18}O_{seawater}$ values in the Pacific were distinctly less than those of the Atlantic. Across the MPT, deep ocean glacial $\delta^{18}O_{seawater}$ increased in both ocean basins but the deep Pacific values increased more than those of the deep Atlantic (Fig. 7c). After 930 ka, glacial deep-water temperature and $\delta^{18}O_{seawater}$ values from the Atlantic and Pacific were more similar.

Deep-water temperatures at Site 1094 in the Atlantic sector of the Southern Ocean (Hasenfratz et al., 2019) are similar to those of the deep Pacific (Fig. S9), but slightly warmer consistent with the modern temperature difference between the two sites. No substantial change in glacial temperatures occurred at Site 1094 across the MPT (Fig. S9). The $\delta^{18}O$ values of seawater at Site 1094 are more similar to those of the deep North Atlantic record. Prior to the MPT, a gradient in $\delta^{18}O_{seawater}$ existed between Site 1094 and the deep Pacific, whereas the values converge after 930 ka.

All five records were stacked to produce global signals of deep ocean temperature (>2500 m) and $\delta^{18}O_{seawater}$ change. The MDOT stack (Fig. S11c) shows a modest gradual decrease in glacial deep-water temperatures from ~1050 to 925 ka primarily related to cooling in the deep North Atlantic. At ~930 ka, the global mean $\delta^{18}O_{seawater}$ stack (Fig. S11b) increases abruptly. This change is more pronounced in ocean volume-weighted records because of the proportionally greater influence of Pacific deep ocean temperature, which shows a warming from MIS 24 through 22 (Figs. 8 and S11). Mean glacial $\delta^{18}O_{seawater}$ values in the ocean volume-weighted stack increase from 0.38 ± 0.08 ‰ prior to ~930 ka to 0.80 ± 0.11 ‰ thereafter, representing a mean difference of ~0.42 ‰ that is statistically significant ($p < 0.001$).

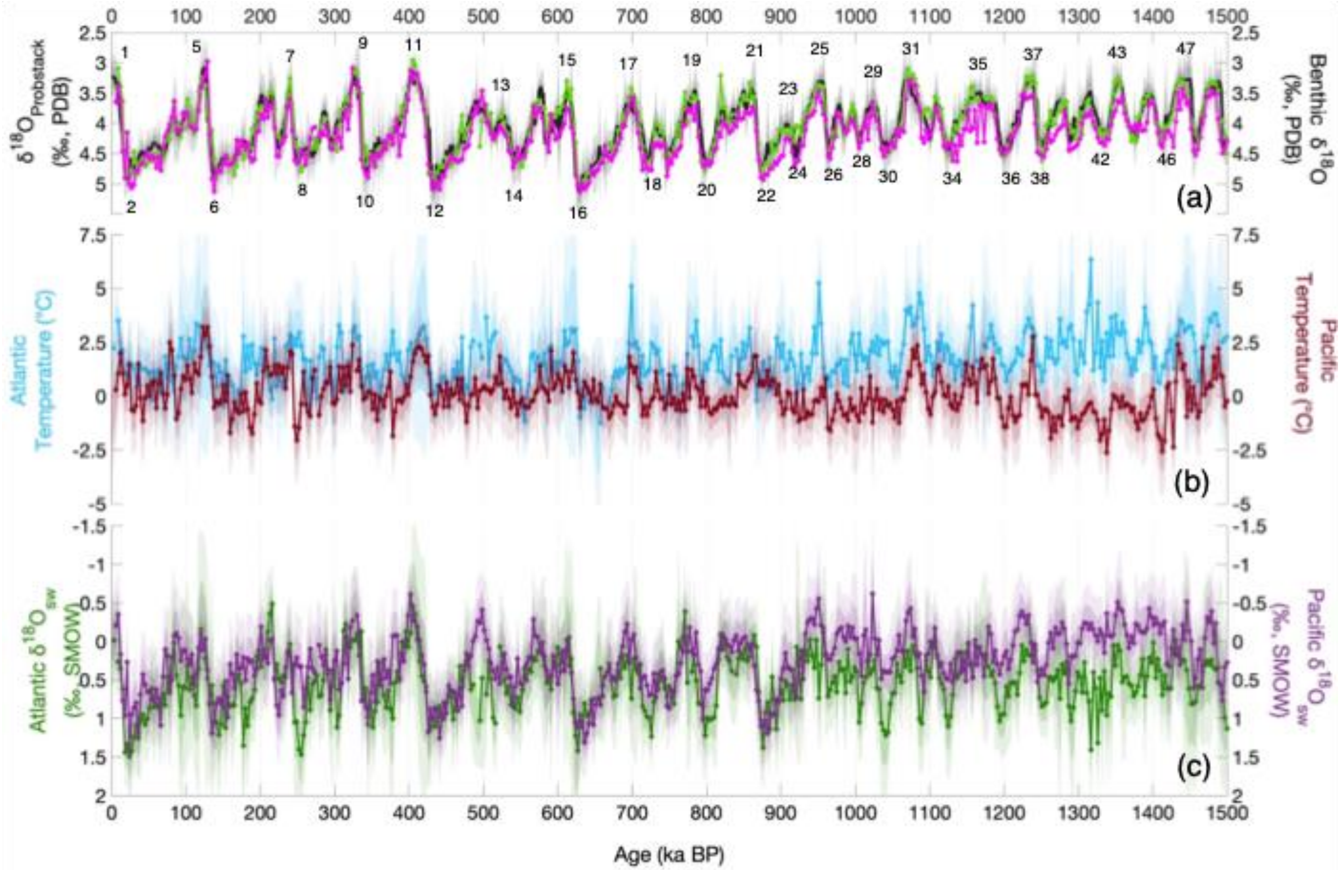

Figure 7: Comparison of North Atlantic and Pacific Ocean deep-water temperature and benthic $\delta^{18}O_{seawater}$ stacks. (a) Prob-stack benthic $\delta^{18}O$ (Ahn et al., 2017) (black line), overlain with contributing benthic $\delta^{18}O$ records for the Atlantic (this study and (Ford et al., 2016; Sosdian and Rosenthal, 2009)) (bright green) and Pacific (Elderfield et al., 2012; Ford and Raymo, 2020) (bright pink) stacks in (b and c). MIS numbers denote glacial (even) and interglacial (odd) stages. (b) Stacked deep-water temperatures for the Pacific (red) and North Atlantic (blue) with dark and light shading indicating 1 and 2σ uncertainties respectively. (c) Stacked deep-water $\delta^{18}O_{seawater}$ for the Pacific (purple) and North Atlantic (green) with uncertainties as in b. Stacks and associated uncertainties represent mean of manually aligned, interpolated (3 kyr resolution) and bootstrapped records, with uncertainties reflecting both analytical error and the spread between paired estimates (see Sect. 2.6).

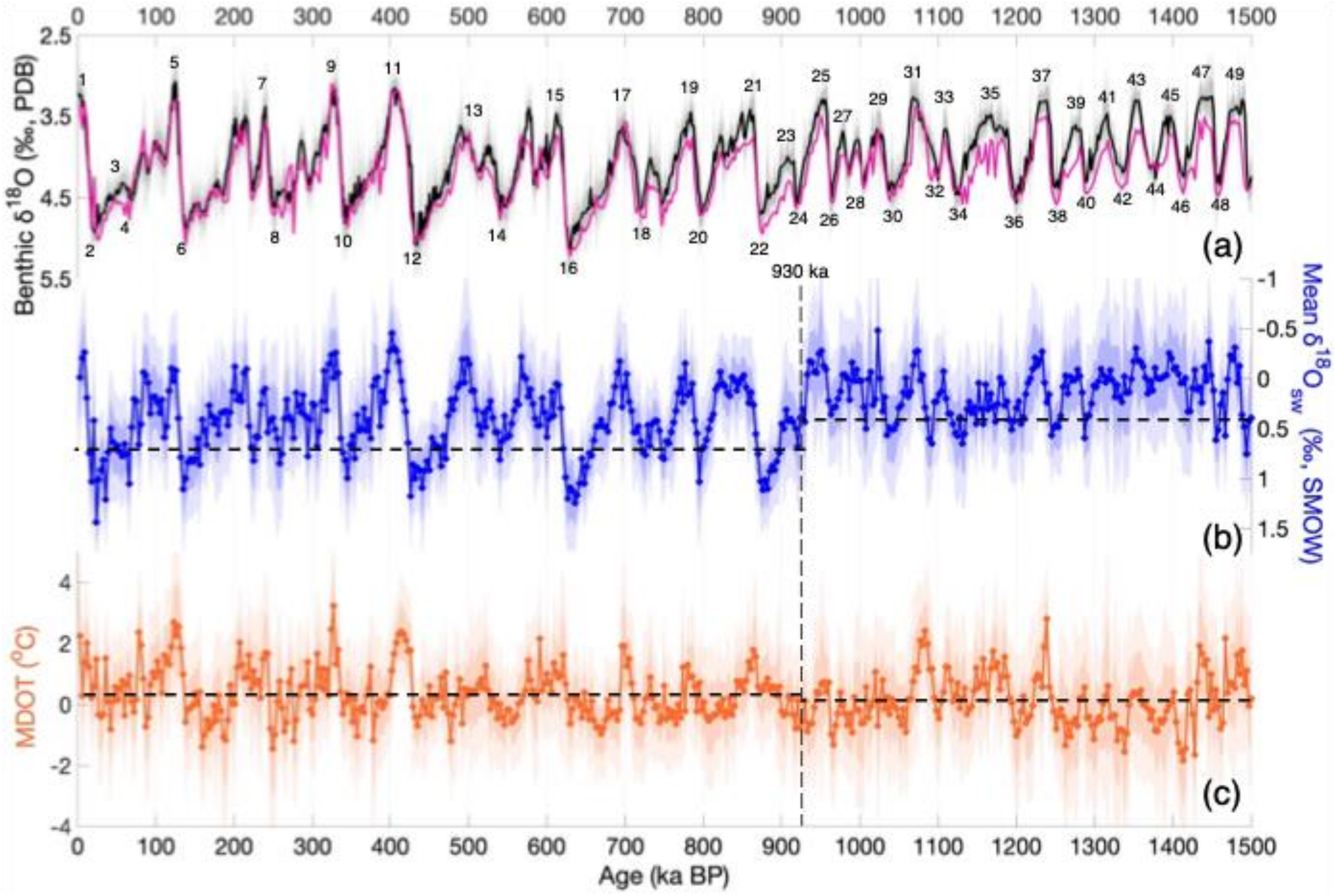

Figure 8: MDOT and mean $\delta^{18}O_{seawater}$ stacks weighted by ocean-basin volume. (a) Basin-volume–weighted benthic $\delta^{18}O$ stack compiled from Atlantic, Pacific and Southern Ocean records used in this study (pink) overlaid on Prob-stack benthic $\delta^{18}O$ (Ahn et al., 2017) (black). MIS numbers denote glacial (even) and interglacial (odd) stages. (b) Globally distributed basin-volume–weighted mean deep-water $\delta^{18}O_{seawater}$ stack (blue). Horizontal dashed lines indicate the glacial mean values for intervals before and after 930 ka. (c) Ocean volume–weighted MDOT stack (orange); the horizontal dashed lines indicate the total mean values for the intervals before and after 930 ka. The vertical dashed line marks 930 ka. Ocean-basin volume weighted stacks were constructed following the approach of Lisiecki and Stern (2016) (Sect. 2.6). Uncertainty envelopes incorporate analytical, calibration and age uncertainties propagated through a Monte Carlo framework, with basin-scale uncertainty additionally reflecting inter-record variability.

4 Discussion

4.1 Basinal differences in abyssal temperature and salinity

Although the deep Atlantic and Pacific stacks contain only two records each, we suggest they are broadly representative of deep-water mass properties in the two basins. Comparison of Atlantic and Pacific temperature and $\delta^{18}O_{seawater}$ records indicate differences in the magnitude of temperature and $\delta^{18}O_{seawater}$ changes across the MPT (Fig. 7b, c). The deep North Atlantic cooled during glacials between ~1050 to 925 ka whereas the deep Pacific remained cold, both before and after the MPT. The cooling in the deep North Atlantic is supported by a decrease (~2 °C) in high-latitude North Atlantic sea surface temperature (SST) at Site 982 on the Rockall Plateau (58° N, 16° W), close to the source area of deep-water formation (Lawrence et al., 2009) (Fig. 9b). Because deep water derived from the Southern Ocean is colder than that sourced from the North Atlantic, part of the cooling may also result from an expansion of southern sourced water into the deep North Atlantic during glacial stages. Cooling coincides with an abrupt increase in neodymium isotopes (εNd) at Site 607 that has been previously interpreted as indicating an increased contribution of Southern Component Water (SCW) in the deep Atlantic (Kim et al., 2021a; Pena and Goldstein, 2014) (Fig. 9d), with similar deep circulation changes inferred for the Pacific (Li et al., 2026) An increase in the $\delta^{13}C$ gradient between the intermediate and deep North Atlantic also supports a greater proportion of SCW in the North Atlantic across the MPT (Fig. 9e) (Lang et al., 2016; Lisiecki, 2014). Neodymium isotope changes in the Atlantic have alternatively been interpreted to represent changes in the end-member Nd value of NCW alongside more modest circulation changes (Pöppelmeier et al., 2020, 2022; Williams et al., 2024; Zhao et al., 2019).

Cooling of Northern Component Water (NCW) would increase its density and create a stratification inversion with deeper water masses in the absence of a density increase of SCW (Knorr et al., 2021). The $\delta^{18}O_{seawater}$ in both the deep North Atlantic and Pacific increases across the MPT reflecting expansion of continental ice sheets, but the increase is greater in the Pacific than the Atlantic (Fig. 7c). We attribute the greater increase in Pacific $\delta^{18}O_{seawater}$ to an increase in the salinity and density of SCW, which may have shoaled the boundary between NCW and SCW in the deep Atlantic if the density contrast between the two water masses increased (Figs. 9c and e) (Song et al., 2025). Glacial-interglacial change in the global ocean density stratification in much of the deep ocean (>2000 m) is controlled by surface freshwater forcing in the Southern Ocean (Sun et al., 2016). Increased salinity can be achieved by decreasing meltwater input to the marginal seas around Antarctica (e.g. Weddell and Ross Seas) either from the Antarctic ice sheet and/or grounded ice shelves. Sea ice expansion around Antarctica also raises salinity through brine rejection and expands the depth range of SCW (Ferrari et al., 2014), but sea ice formation does not significantly alter the $\delta^{18}O_{seawater}$ of seawater (Kim and Timmermann, 2024; Toyota et al., 2013).

Raymo et al. (2006) suggested the East Antarctic ice sheet was terrestrial-based with melting margins before the MPT and transformed to a marine-based ice sheet afterward, which would have decreased meltwater to marginal seas. An unconformity in the Ross Sea Embayment that spans the MPT has been interpreted to represent widespread expansion of a marine-based ice sheet (McKay et al., 2012) into the Ross Sea where AABW is formed today. Adkins (2013) proposed that cooling of NADW during glacial stages of the late Pleistocene decreased melting rates of floating Antarctic ice shelves. Adkins (2013) suggested decreased meltwater input led to the formation of a cold and salty version of Antarctic Bottom Water, and this water mass filled the deep ocean basins. We observe cooling of the high-latitude and deep North Atlantic across the MPT at the same time as the inferred salinity increase of the deep Pacific, which may support the mechanism outlined by Adkins (2013).

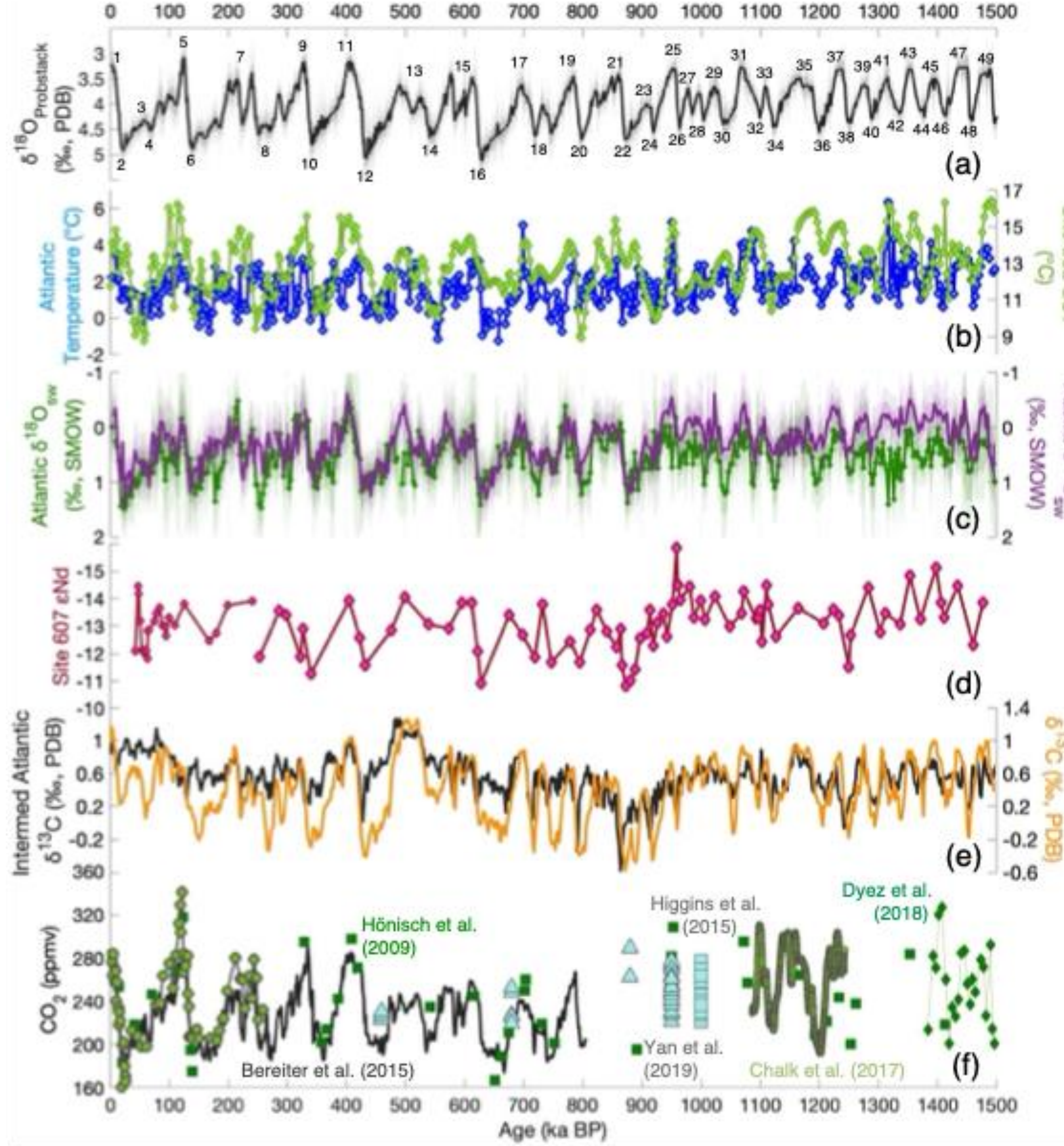

Figure 9: Comparison of deep-water temperature, salinity, ocean circulation and atmospheric $p\mathrm{CO_2}$ records over the last 1.5 Ma. (a) Benthic δ^{18}O Prob-stack (Ahn et al., 2017) (black line), MIS numbers denote glacial (below) and interglacial (above) stages. (b) Alkenone $\mathrm{U^{k'}_{37}}$-derived, sea surface temperature (SST) record from ODP Site 982 (Lawrence et al., 2009) (green line with markers) overlaying the Atlantic stack for deep-water temperature (this study; blue line with markers). (c) Atlantic (green) and Pacific (purple) $\delta^{18}\mathrm{O_{seawater}}$ stacks (this study). (d) DSDP Site 607/V30-97 εNd proxy for North Atlantic Ocean circulation changes (Kim et al., 2021b) (dark pink line with pink diamonds). (e) Carbon isotope gradient between regional δ^{13}C stacks (Lisiecki, 2014) for the intermediate depth North Atlantic (black) and middle deep Atlantic (orange). Low δ^{13}C reflects reduced ventilation in the deep Atlantic. (f) Atmospheric $p\mathrm{CO_2}$ records (presented as in (Thomas et al., 2022)): Antarctic 800-kyr ice core data (Bereiter et al., 2015) (black line); Allan Hills Blue Ice (blue triangles (Yan et al., 2019) and blue squares (Higgins et al., 2015)); and δ^{11}B-based reconstructed $p\mathrm{CO_2}$ [(Dyez et al., 2018) green line with diamonds; (Hönisch et al., 2009) solid green squares; (Chalk et al., 2017) early Pleistocene light green line/small circles, and late Pleistocene light green circles]. Chronology for Atlantic and Pacific stacks is available in Sect. 2.1, all other records are presented on their original timescales.

The freshwater fluxes to marginal seas can also be decreased by exporting freshwater to lower latitude via icebergs discharge and sea ice (Ferrari et al., 2014; Jansen, 2017). Starr et al. (2021) reported an increase in IRD in the Subantarctic Zone across the MPT and suggested this reflected increased transport of meteoric freshwater away from Antarctica. This process could have contributed to increased salinity in source areas of SCW formation, especially in the Weddell Sea sector. At the same time, increased transport of icebergs and sea ice from Antarctica increased the freshwater flux to the subantarctic, strengthened the halocline and slowed deep-to-surface exchange that controls carbon dioxide release to the atmosphere (Hasenfratz et al., 2019).

4.2 Implications for carbon storage

Although we cannot pinpoint which of the many processes discussed above was responsible for increased salinification and densification of SCW— some or all may have contributed— increased stratification of the glacial deep ocean may have played a role in enhancing ocean carbon storage and lowering atmospheric pCO_2 concentrations (Adkins 2013). Increased deep ocean stratification provides a physical mechanism by which sinking organic carbon can be remineralised and accumulate in the deep sea. In the process, oxygen is consumed, nutrients are released and total dissolved inorganic carbon (DIC) increases, although carbonate ion decreases. Several studies have reported an increase in deep-sea nutrients and lowered carbonate ion and oxygen concentrations in the deep Atlantic (e.g. (Fig. 9e) (Farmer et al., 2019; Lear et al., 2016; Lisiecki, 2014; Thomas et al., 2022) and Pacific (Diz et al., 2020; Peng et al., 2026; Qin et al., 2022) across the MPT.

Increased stratification of the deep ocean by itself is insufficient to change deep-ocean carbon storage. The biological pump exports organic matter from the surface ocean that is remineralised at depth. In the Southern Ocean, biological export production is thought to have increased owing to iron fertilization from dust over the MPT (Martínez-Garcia et al., 2011). The return of deep water towards the surface in the upwelling region of the Antarctic Circumpolar Current (ACC) ventilates the deep ocean through gas exchange in the Southern Ocean. This surface/deep exchange of water was reduced (“isolated”) during glacial periods because of a strengthened halocline and reduced upwelling (Sigman et al., 2021). At Site 1094 across the MPT, Hasenfratz et al. (2019) suggested a reduction in deep water supply to the surface and a concomitant freshening of surface waters that strengthened the halocline, thereby reducing carbon dioxide release to the atmosphere. The strength of the Westerlies and ACC are also important for the upwelling of deep-water masses from the ocean interior in the Antarctic Zone, although changes may be asynchronous in different sectors of the Southern Ocean (Lamy et al., 2024; Sun et al., 2016).

Most hypotheses and models to explain the MPT invoke a glacial atmospheric pCO_2 decline to promote the growth of larger ice sheets; indeed, it's difficult to explain the MPT without this radiative cooling especially in the tropics (Herbert, 2023). Some studies have indicated a modest drop (~20 ppm) in concentrations of glacial atmospheric pCO_2 across the (Chalk et al., 2017; Higgins et al., 2015; Hönisch et al., 2009; Yan et al., 2019) (Fig. 9f), whereas others have found no mean change (Marks-Peterson et al., 2026). The uncertain magnitude of atmospheric pCO_2 decline across the MPT underscores the critical importance of new data from the BE-OI core, which has recovered continuous ice to 1.2 Ma and possibly to 1.5 Ma (Barbante etal., 2025).

4.3 Mean Deep Ocean Temperature

A critical question for the MPT is by how much and how fast did global deep ocean temperature and ice volume change? Global stacking of mean deep ocean temperature and $\delta^{18}O_{seawater}$ records (derived from paired benthic Mg/Ca-$\delta^{18}O$) can address this question and be compared to other more indirect approaches of estimating temperature and ice volume changes from benthic $\delta^{18}O$ records. Although only 5 long records of tandem benthic $\delta^{18}O$–Mg/Ca measurements exist spanning the last 1.5 Myr, we stacked the records first with equal weighting to reconstruct global records and then weighted by the volumes of different ocean basins (Lisiecki and Stern, 2016) (Sect. 2.6) to better estimate global averages. Whereas the unweighted glacial MDOT record shows a slight decrease after ~900 ka, it is biased by the cooling of the deep Atlantic at Site 607 (Fig. S11c). Considering the much smaller volume of the deep North Atlantic compared to the deep Pacific, the volume-weighted MDOT stack is more representative and shows minimal change across the MPT (Fig. 8c).

We compare our stacked MDOT record with similar estimates derived by other methods. Rohling et al. (2021) (R21) calculated deep-sea temperatures (DST) using benthic $\delta^{18}O$ and estimates of $\delta^{18}O_{seawater}$ from sea level reconstructions. Our changes in MDOT agree well with R21 older than 1200 ka, after which the amplitude of R21 is greater than our MDOT (Fig. 10a). Neither record shows substantial cooling of deep ocean temperatures across the MPT. Chandler and Langebroek (2024) similarly used benthic $\delta^{18}O$, Mg/Ca and sea level reconstructions to estimate changes in mean Circumpolar Deep Water temperature (MCDWT) for the past 800 ka, including Sites 1123 and 1094 but using slightly different calibrations than this study (Fig. 10b). For the last 800 kyrs, our MDOT agrees well with MCDWT, indicating the slightly different approaches yield similar results. Lastly, we compare our MDOT estimates with changes in mean ocean temperature (MOT) reconstructed using noble gas (Xe/Kr) from the EPICA ice core (Grimmer et al., 2025) and shallow ice cores recovered from the Allan Hills blue ice area, Antarctica (Shackleton et al., 2026) (Fig. 10c). The latter likely records a weighted averaging of glacial and interglacial conditions. There is good agreement between the two, especially considering that our MDOT does not include the entire ocean recorded by noble gas MOT. Both records show little change in MDOT or MOT across the MPT (Shackleton et al., 2026).

Both our MDOT and the noble gas MOT (Shackleton et al., 2026) results differ from reconstructions of Clark et al. (2024, 2025), which are based on using global mean sea surface temperatures (ΔGMSST) to estimate ΔMOT (Wolff, 2026). The ΔGMSST estimates are converted to ΔMOT using a non-constant ratio of ΔMOT/ΔGMSST over the MPT. For the period from 1.5 to ~0.9 Ma, these estimates give warmer deep-water temperatures relative to our study, followed by a marked cooling in deep ocean temperature (>2000 m) at ~900 ka (Fig. 10d). The Clark et al. compilation is strongly biased towards the deep North Atlantic (predominantly Site 607) with comparatively sparse Pacific deep ocean temperature (>2000 m) data over this interval (Clark et al., 2025; Lear et al., 2003). Site U1385 does not show cooling between 1.5 to ~0.9 Ma but the records from

Sites 607 show a 1 °C long term cooling trend, which is unlikely to represent a global mean change in deep-ocean temperature (Figs. 2b, 3b, c, 5b, S3a, and S7b, c; Sect. 3.1). Instead, our findings support previous interpretations for near-freezing glacial bottom water temperatures in the Pacific and the South Atlantic Southern Ocean throughout the period from 1.5 to ~0.9 Ma, with no substantial change across the MPT (Elderfield et al., 2012a; Ford and Raymo, 2020; Hasenfratz et al., 2019; Siddall et al., 2010) (Figs. 8c, S9c and S12c). These results appear to be consistent with recent ice core noble gas-based reconstructions of MOT (Shackleton et al., 2026) (Fig. 10c), but higher resolution MOT data from BE-OI are needed to capture the full amplitude of glacial-interglacial variations (Barbante et al., 2025).

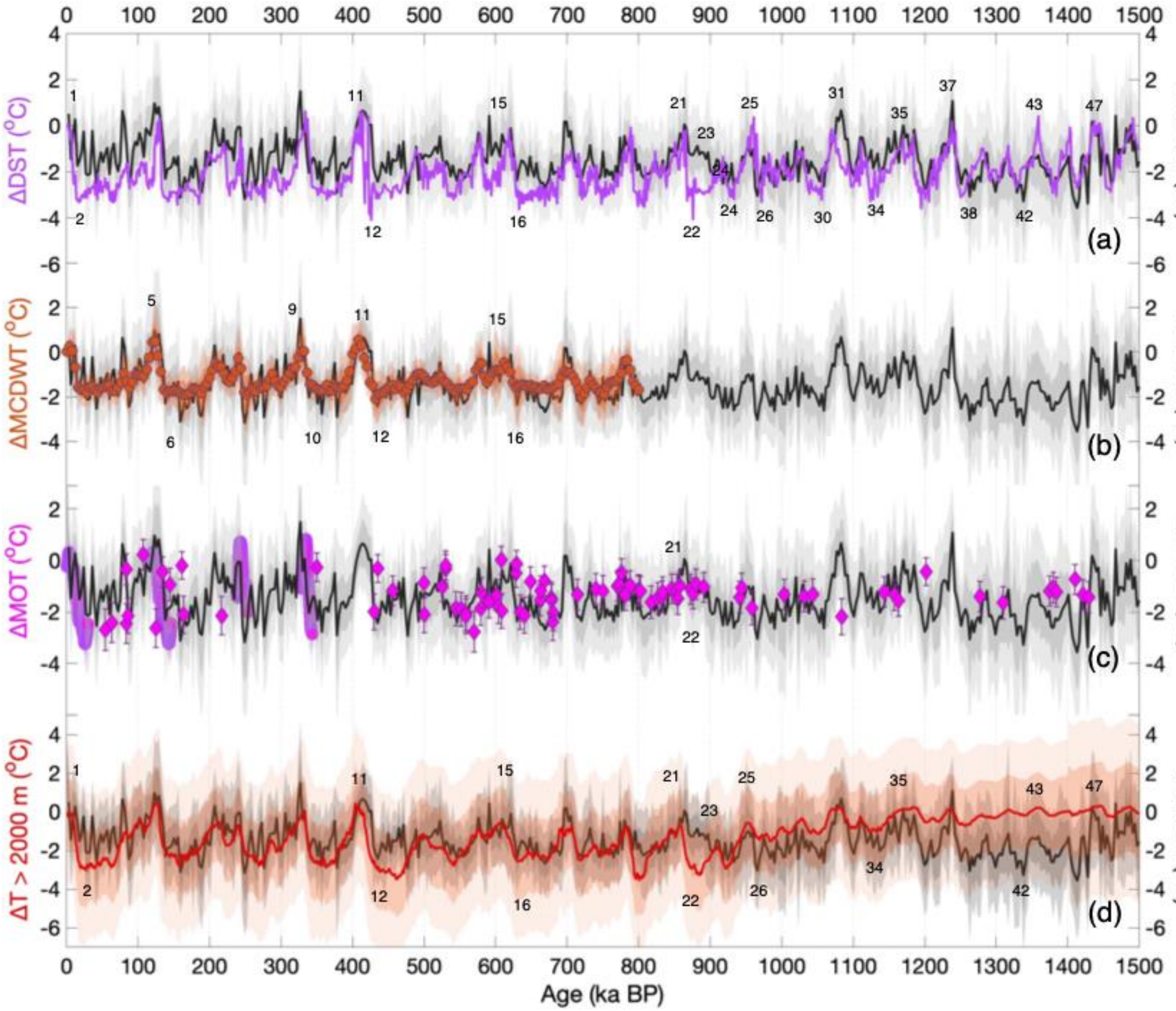

Figure 10: Comparison of MDOT with similar mean ocean and deep-water temperature reconstructions. All panels show the change in volume-weighted MDOT (ΔMDOT) (this study; black line) relative to an average present day value (1.73 ºC) versus: (a) the change in deep-sea temperature (ΔDST) estimated relative to the present (Rohling et al., 2021) (purple line); (b) the change in mean CDW temperature (ΔMCDWT) relative to present (Chandler and Langebroek, 2024) (dark orange circles); (c) the change in MOT (ΔMOT) derived from noble gas measurements in ice cores (Grimmer et al., 2025) (purple and pink circles) and, in Allan Hills blue ice (pink diamonds) (Shackleton et al., 2026), error bars on individual MOT estimates represent absolute uncertainties; and, (d) ΔMOT inferred from ΔGMSST and proxy-based deep-water temperature (Clark et al., 2025) (red), with both records referenced to the Early Holocene (0 °C at 10 ka) and offset by -1.73 0 °C following (Clark et al., 2025). Dark and light shading of the same colour represent 1σ and 2σ uncertainty envelopes, respectively. Uncertainties associated with ΔMOT are taken directly from the published datasets of Clark et al. (2025). MIS numbers mark many of the glacial (even) and interglacial (odd) stages.

4.4 Mean $\delta^{18}O_{seawater}$ and Ice Volume

Both weighted and unweighted mean ocean $\delta^{18}O_{seawater}$ stacks were compiled and show a step-like increase across the MPT at 930 ka (Figs. 8b and S11b), supporting previous interpretations of increased continental ice volume during most glacial periods after ~900 ka (Elderfield et al., 2012; Ford and Raymo, 2020). Our volume-weighted mean $\delta^{18}O_{seawater}$ stack is consistent with process-based estimates of $\delta^{18}O_{seawater}$ over the past 1.5 Myr (Rohling et al., 2021) (Fig. 11a) and with reconstructions of relative sea level (RSL) change for the past ~500 ka (Grant et al., 2012, 2014) (Fig. 11b). However, our value for MIS 22 is considerably greater than R21. This is the result of a warming trend of MDOT during MIS 22 that yields greater $\delta^{18}O_{seawater}$ values when the signal is deconvolved from the benthic $\delta^{18}O$ of calcite. Deep North Pacific Site 1208, in particular, shows anomalously high temperatures during MIS 22 that contribute to this discrepancy.

Our results diverge from (Clark et al., 2024, 2025) in that our $\delta^{18}O_{seawater}$ values are lower prior to the MPT, particularly in the interval older than 1200 kyrs, suggesting less glacial ice volume before the MPT. They infer surprisingly large ice sheets before the MPT and relatively little change at ~900 ka, which is contrary to our results and most previous studies (Bintanja and Van De Wal, 2008; Clark et al., 2006; Elderfield et al., 2012a; Ford and Raymo, 2020; Rohling et al., 2021). Their method of reconstruction discounts the temperature and $\delta^{18}O_{seawater}$ records from Pacific Sites 1123 and 1208 (Elderfield et al., 2012; Ford and Raymo, 2020) claiming they are unrepresentative of global values and reflect regional hydrographic changes. While we agree there is a hydrographic (salinity) component to the increase in the glacial deep Pacific $\delta^{18}O_{seawater}$ signal that exceeds the Atlantic signal, there is also a global increase in $\delta^{18}O_{seawater}$ reflecting greater ice volume across the MPT.

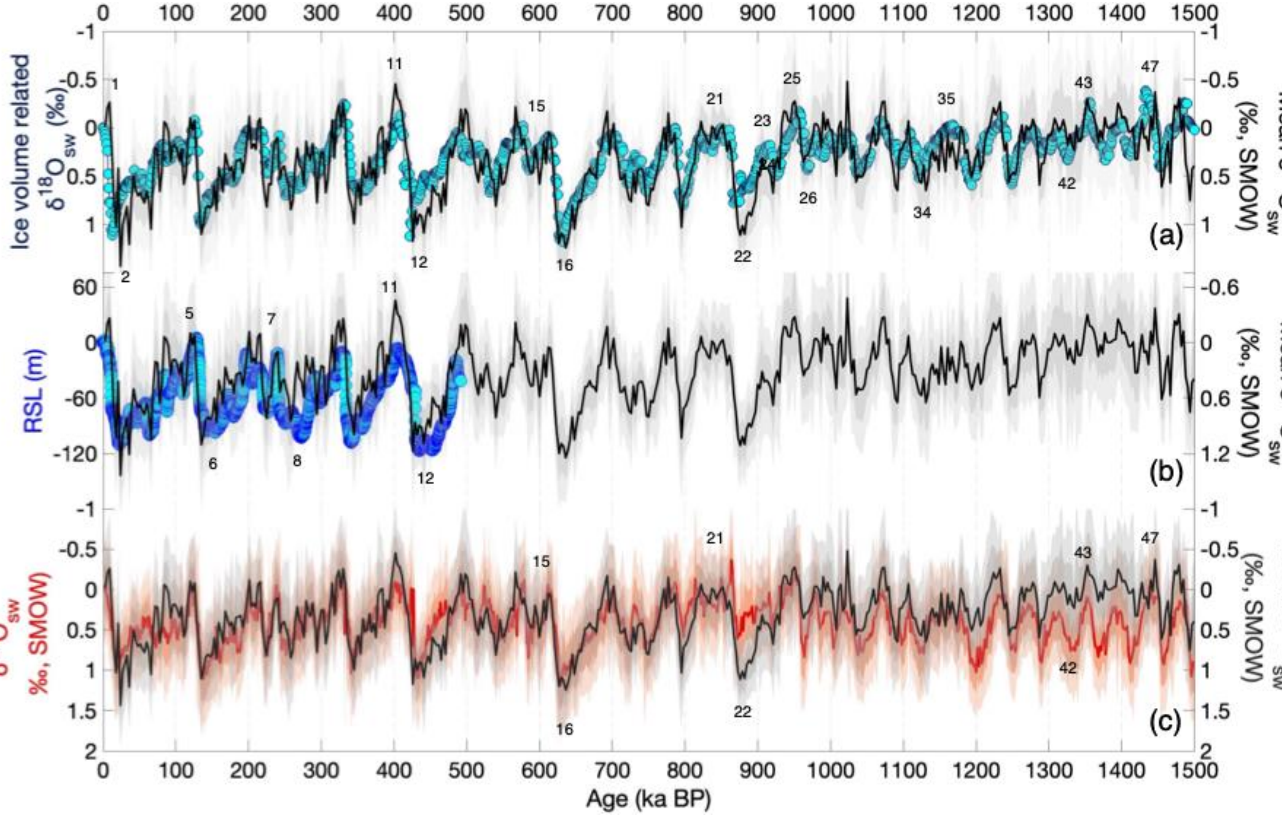

Figure 11: Comparison of mean $\delta^{18}O_{seawater}$ with similar process-based and relative sea level reconstructions. Volume-weighted mean $\delta^{18}O_{seawater}$ stack shown in each panel (this study; black) is compared against: (a) process-based estimated ice-volume related deep-sea $\delta^{18}O_{seawater}$ (Rohling et al., 2021) (light blue circles); (b) Red Sea relative sea level (RSL) reconstructions (Grant et al., 2012, 2014) (dark and light blue circles) scaled so that $\delta^{18}O_{seawater}$ of 1.0 ‰ is equivalent to 10 m RSL; and, (c) $\delta^{18}O_{seawater}$ derived from the deconvolution of the benthic $\delta^{18}O$ Prob-stack using inferred changes in MOT (Clark et al., 2025) (red). MIS numbers denote glacial (below) and interglacial (above) stages. Dark and light shading of the same colour represent 1σ and 2σ uncertainty envelopes, respectively. Uncertainties associated with $\delta^{18}O_{seawater}$ are taken directly from the published datasets of Clark et al. (2025). The $\delta^{18}O_{seawater}$ reconstruction of Clark et al. (2025) includes removal of a long-term increase of 0.083 ‰ Myr^{-1} in benthic $\delta^{18}O$, which is not applied to our records because such an arbitrary adjustment for diagenesis remains unproven. This adjustment is small relative to uncertainties in the $\delta^{18}O_{seawater}$ compilations and would increase the divergence between the two mean $\delta^{18}O_{seawater}$ curves.

4.5 Limitations and Future Opportunities

The small number of long, continuous benthic Mg/Ca–$\delta^{18}O$ records available across the MPT leads to questions about how well they represent basin-wide or global averages. Low abundance of preferred benthic foraminiferal taxa in some of the records results in time gaps where fewer than 5 sites are available for stacking. The water depths of the studied sites are all below 2500 mbsl and a greater depth range would provide a better comparison with noble gas-based MOT estimates across the MPT (Shackleton et al., 2026). The temporal resolution is relatively low (3 kyrs) and may not reflect the full amplitude of changes and certainly do not capture millennial-scale variability. Complementary B/Ca on the same samples would provide a proxy for carbonate ion changes, which could be used to assess if Mg/Ca palaeotemperatures of different benthic species of foraminifera have been affected by dissolution. The propagation of error when using paired benthic Mg/Ca–$\delta^{18}O$ to calculate the $\delta^{18}O_{seawater}$ is fairly large (±0.24 ‰ for *U. peregrina* and ±0.16 ‰ for *G. affinis* (1 σ), with the dominant contribution arising from temperature uncertainty). Using benthic foraminifera taxa with a greater sensitivity of Mg/Ca to temperature could potentially reduce the errors (Yang et al., 2025).

The recent recognition that the time rate of change of benthic $\delta^{18}O$ is a proxy for Earth's Energy Imbalance (EEI) offers the opportunity to investigate the processes that modify the global energy budget on long timescales (Shackleton et al., 2023). With more records, the derivative of the deconvolved stacks would permit separation of the sensible and latent heat components and provide valuable insight how the Earth's energy balance changed during the MPT.

All of the points discussed above underscore the importance of acquiring additional paired benthic Mg/Ca–$\delta^{18}O$ records to improve the records presented herein. Furthermore, the proposed causes for the changes in deep-ocean stratification and their impact on deep-ocean carbon storage should be tested with numerical models.

5 Conclusions

The causes of the MPT have been sought since it was first recognized in oxygen isotope records over 50 years ago (Pisias and Moore, 1981; Shackleton, Nicholas John and Opdyke, 1973). The MPT involved a fundamental change in the interaction of deep-ocean circulation, atmospheric pCO_2, and the cryosphere that permitted continental ice sheets to grow large enough that they were able to survive modest rises in summer insolation that would have resulted in deglaciation prior to the MPT (Ganopolski, 2024; Raymo et al., 1997; Willeit et al., 2019). Here we suggest that the MPT involved changes in the physical properties of the abyssal ocean, including a cooling of the deep North Atlantic and salinification of the deep water in the Pacific. This resulted in increased density stratification of the deep ocean in glacial periods after ~900 ka.

Global ocean density stratification in much of the deep ocean (>2000 m) is controlled by surface freshwater forcing in the Southern Ocean (Sun et al., 2016). We suggest that across the MPT, meltwater input to the marginal seas around Antarctica decreased and sea ice increased during glacial periods, resulting in formation of cold (near freezing), salty deep water. Increased deep ocean stratification provides a physical mechanism by which sinking organic carbon from the surface can accumulate in the deep sea, especially if accompanied by increased export production and surface stratification in the Southern Ocean. Many complementary studies support increased carbon storage in the deep Atlantic (e.g. (Fig. 9e) (Farmer et al., 2019; Lear et al., 2016; Lisiecki, 2014; Thomas et al., 2022) and Pacific (Diz et al., 2020; Peng et al., 2026; Qin et al., 2022a) across the MPT, and some atmospheric pCO_2 proxy records show a moderate decline in glacial atmospheric concentrations (Chalk et al., 2017; Higgins et al., 2015; Hönisch et al., 2009; Yan et al., 2019). Forthcoming analyses of the newly recovered continuous

Antarctic ice core spanning the MPT (Wolff et al., 2022) will provide critical information on changes in greenhouse gases and MOT, which are needed to test many of the inferences made herein.

Data availability. All data, not previously reported, has been deposited at the World Data Center PANGAEA repository (www.pangaea.de.) and will be publicly available when the paper is accepted and a DOI issued
Previously reported benthic $\delta^{18}O$ for IODP Site U1385 (Hodell et al., 2023) are archived at: (https://doi.org/10.1594/PANGAEA.951401).

Supplement link.

Author contributions. Conceptualization: DAH conceived the study, led its design, and collected the samples; NCT co-designed the study: NCT and MG processed and prepared the new dataset; NCT organised the complete dataset and associated metadata for analysis and archiving. Formal analysis: NCT and HLF applied statistical and computational methods to analyse the data and develop the stacked reconstructions. Funding acquisition: DAH. Investigation: NCT and MG, collected new trace element data from Site U1385; NCT and DAH generated the stable isotope data; all authors contributed to data analysis. Methodology: DAH and NCT. Project administration: NCT and DAH coordinated the research activities and workflow. Resources: DAH and MG provided laboratory facilities, materials and analytical support. Software: HLF and NCT implemented and executed the PSU Solver code. Visualization: NCT and DAH. Writing – original draft: NCT and DAH. Writing – review and editing: NCT, MG, HLF, and DAH.

Competing interests. One of the (co-)authors is a member of the editorial board of Climate of the Past. The authors declare that they have no other competing interests.

Disclaimer. Publisher's note:

Acknowledgements. We thank all members of the Godwin laboratory for Palaeoclimate Research in the Department of Earth Science, University of Cambridge, UK for technical assistance: J. Booth and M Mleneck-Vautravers for selection and preparation of samples for stable isotope analysis; J. Rolfe and J. Nicolson for performing stable isotope analyses; J. Nicolson and M. Mleneck-Vautravers for much of the preparation of samples for trace element spectrophotometry and conducting ICP-OES analyses. The International Ocean Discovery Program (IODP) provided samples used in this research. We are thankful to the crew of the *JOIDES Resolution* during IODP Expedition 339 including the drilling crew, ship's crew, and scientific and technical staff who made core recovery from Site U1385 possible.

Financial support. The Natural Environment Research Council (NERC) provided funding to DAH to collect IODP and JC089 samples and for all laboratory and analytical costs. NERC grants NE/R000204/1 and NE/K005804/1 (to DAH). NCT has been privately funded by R. M. Thomas.

Review statement. included by Copernicus.

References

Adkins, J. F.: The role of deep ocean circulation in setting glacial climates, Paleoceanography, 28, 539–561, https://doi.org/10.1002/palo.20046, 2013.

Ahn, S., Khider, D., Lisiecki, L. E., and Lawrence, C. E.: A probabilistic Pliocene–Pleistocene stack of benthic $\delta^{18}O$ using a profile hidden Markov model, Dyn. Stat. Clim. Syst., 2, 1–16, https://doi.org/10.1093/climsys/dzx002, 2017.

An, Z., Zhou, W., Zhang, Z., Zhang, X., Liu, Z., Sun, Y., Clemens, S. C., Wu, L., Zhao, J., Shi, Z., Ma, X., Yan, H., Li, G., Cai, Y., Yu, J., Sun, Y., Li, S., Zhang, Y., Stepanek, C., Lohmann, G., Dong, G., Cheng, H., Liu, Y., Jin, Z., Li, T., Hao, Y., Lei, J., and Cai, W.: Mid-Pleistocene climate transition triggered by Antarctic Ice Sheet growth, Science, 385, 560–565, https://doi.org/10.1126/science.abn4861, 2024.

Barbante, C. and the Beyond EPICA Team: Beyond EPICA – Oldest Ice Core: Insights from a 1.2-Million-Year-Old Climate Record, EGU General Assembly 2025, Vienna, Austria, 27 Apr–2 May 2025, EGU25-10358, https://doi.org/10.5194/egusphere-egu25-10358, 2025.

Barker, S., Greaves, M., and Elderfield, H.: A study of cleaning procedures used for foraminiferal Mg/Ca paleothermometry, Geochem, Geophys. Geosyst., 4, 1–20, https://doi.org/10.1029/2003GC000559, 2003.

Basak, C., Kapuge, A. K. I. U., Farmer, J. R., Symes, E., Middleton, J. L., Gottschalk, J., Arz, H. W., Lamy, F., Winckler, G., and Cruz, A. P. S.: Southern Hemisphere initiation of the mid-Pleistocene transition, Sci. Adv., 12, eaea6811, https://doi.org/10.1126/sciadv.aea6811, 2026.

Bereiter, B., Eggleston, S., Schmitt, J., Nehrbass-Ahles, C., Stocker, T. F., Fischer, H., Kipfstuhl, S., and Chappellaz, J.: Revision of the EPICA Dome C CO_2 record from 800 to 600 kyr before present, Geophys. Res. Lett., 42, 542–549, https://doi.org/10.1002/2014GL061957, 2015.

Berends, C. J., Köhler, P., Lourens, L. J., and van de Wal, R. S. W.: On the cause of the mid-Pleistocene transition, Rev. Geophys., 59, 1–20, https://doi.org/10.1029/2020RG000727, 2021a.

Berends, C. J., de Boer, B., and van de Wal, R. S. W.: Reconstructing the evolution of ice sheets, sea level and atmospheric CO_2 during the past 3.6 million years, Clim. Past, 17, 361–377, https://doi.org/doi.org/10.5194/cp-17-361-2021, 2021b.

Berger, A., Li, X. S., and Loutre, M. F.: Modelling NorthernHemisphere ice volume over the last 3 Ma, Quat. Sci. Rev., 18, 1–11, https://doi.org/10.1016/S0277-3791(98)00033-X, 1999.

Billups, K., York, K., and Bradtmiller, L. I.: Water column stratification in the Antarctic Zone of the Southern Ocean during the Mid-Pleistocene Climate Transition, Paleoceanogr. Paleoclimatology, 33, 432–442, https://doi.org/10.1029/2018PA003327, 2018.

Bintanja, R. and van de Wal, R. S. W.: North American ice-sheet dynamics and the onset of 100,000-year glacial cycles, Nature, 454, 869–872, https://doi.org/10.1038/nature07158, 2008.

Birner, B., Hodell, D. A., Tzedakis, P. C., and Skinner, L. C.: Similar millennial climate variability on the Iberian Margin during two early Pleistocene glacials and MIS 3, Paleoceanography, 31, 203–217, https://doi.org/10.1002/2015PA002868, 2016.

Boiteau, R., Greaves, M., and Elderfield, H.: Authigenic uranium in foraminiferal coatings : A proxy for ocean redox chemistry, Paleoceanography, 27, 1–8, https://doi.org/10.1029/2012PA002335, 2012.

Broecker, W. S. and Peng, T. H.: Greenhouse Puzzles: Keeling's World, Eldigio Press, 1998.

Broecker, W. S. and Peng, T. H.: Tracers in the Sea., Eldigio Press, 1982.

Butcher, S., King, T., and Zalewski, L., Apocrita—High Performance Computing Cluster for Queen Mary University of

London: London, Queen Mary University of London Technical Report, 2 p., https://doi.org/10.5281/ze- nodo.438045, 2017.

Chalk, T. B., Hain, M. P., Foster, G. L., Rohling, E. J., Sexton, P. F., Badger, M. P. S., Cherry, S. G., Hasenfratz, A. P., Haug, G. H., Jaccard, S. L., Martínez-García, A., Pälike, H., Pancost, R. D., and Wilson, P. A.: Causes of ice age intensification across the Mid-Pleistocene Transition, Proc. Natl. Acad. Sci., 114, 13114–13119, https://doi.org/10.1073/pnas.1702143114, 2017.

Chalk, T. B., Foster, G. L., and Wilson, P. A.: Dynamic storage of glacial CO_2 in the Atlantic Ocean revealed by boron [CO_3^{2-}] and pH records, Earth Planet. Sci. Lett., 510, 1–11, https://doi.org/10.1016/j.epsl.2018.12.022, 2019.

Chandler, D. M. and Langebroek, P. M.: Glacial-interglacial Circumpolar Deep Water temperatures during the last 800,000 years: estimates from a synthesis of bottom water temperature reconstructions, Clim. Past, 20, 2055–2080, https://doi.org/10.5194/cp-20-2055-2024, 2024.

Chandler, M., Zilberman, N. V, and Sprintall, J.: The Deep Western Boundary Current of the Southwest Pacific Basin : insights from DeepArgo, J. Geophys. Res. Ocean., 129, e2024JC021098, https://doi.org/10.1029/2024JC021098, 2024.

Clark, P. U. and Pollard, D.: Origin of the Middle Pleistocene Transition by ice sheet erosion of regolith, Paleoceanography, 13, 1–9, https://doi.org/10.1029/97PA02660, 1998.

Clark, P. U., Archer, D., Pollard, D., Blum, J. D., Rial, J. A., Brovkin, V., Mix, A. C., Pisias, N. G., and Roy, M.: The Middle Pleistocene Transition: characteristics, mechanisms, and implications for long-term changes in atmospheric pCO_2, Quat. Sci. Rev., 25, 3150–3184, https://doi.org/10.1016/j.quascirev.2006.07.008, 2006.

Clark, P. U., Shakun, J. D., Rosenthal, Y., Köhler, P., and Bartlein, P. J.: Global and regional temperature change over the past 4.5 million years, Science, 383, 884–890, https://doi.org/10.1126/science.adi1908, 2024.

Clark, P. U., Shakun, J. D., Rosenthal, Y., Zhu, C., Bartlein, P. J., Gregory, J. M., Köhler, P., Liu, Z., and Schrag, D. P.: Mean ocean temperature change and decomposition of the benthic $\delta^{18}O$ record over the past 4.5 million years, Clim. Past, 21, 973–1000, 2025.

van Dijk, I., Mouret, A., Oron, S., Evans, D., Boer, W., and Barras, C.: Species-specific offsets in manganeseincorporation inhyaline foraminiferal calcite across a gradient of seawater [Mn], Geochemistry, Geophys. Geosystems, 26, 1–22, https://doi.org/10.1029/2025GC012363, 2025.

Diz, P., Cobelo-García, A., Hernández-Almeida, I., Corbí, H., and Bernasconi, S. M.: Persistent East Equatorial Pacific carbon storage at the Middle Pleistocene Transition, Paleoceanogr. Paleoclimatology, 35, e2019PA003789, https://doi.org/10.1029/2019PA003789, 2020.

Dyez, K. A., Hönisch, B., and Schmidt, G. A.: Early Pleistocene obliquity-scale pCO_2 variability at ~1.5 million years ago, Paleoceanogr. Paleoclimatology, 33, 1270–1291, https://doi.org/10.1029/2018PA003349, 2018.

Elderfield, H., Yu, J., Anand, P., Kiefer, T., and Nyland, B.: Calibrations for benthic foraminiferal Mg/Ca paleothermometry and the carbonate ion hypothesis, Earth Planet. Sci. Lett., 250, 633–649, https://doi.org/10.1016/j.epsl.2006.07.041, 2006.

Elderfield, H., Greaves, M., Barker, S., Hall, I. R., Tripati, A., Ferretti, P., Crowhurst, S., Booth, L., and Daunt, C.: A record of bottom water temperature and seawater $\delta^{18}O$ for the Southern Ocean over the past 440 kyr based on Mg/Ca of benthic foraminiferal *Uvigerina* spp., Quat. Sci. Rev., 29, 160–169, https://doi.org/10.1016/j.quascirev.2009.07.013, 2010.

Elderfield, H., Ferretti, P., Greaves, M., Crowhurst, S. J., McCave, I. N., Hodell, D., and Piotrowski, A. M.: Evolution of ocean temperature and ice volume through the Mid-Pleistocene Climate Transition, Science, 337, 704–709, https://doi.org/10.1126/science.1221294, 2012.

Farmer, J. R., Hönisch, B., Haynes, L. L., Kroon, D., Jung, S., Ford, H. L., Raymo, M. E., Jaume-Seguí, M., Bell, D. B., Goldstein, S. L., Pena, L. D., Yehudai, M., and Kim, J.: Deep Atlantic Ocean carbon storage and the rise of 100,000-year glacial cycles, Nat. Geosci., 12, 350–360, https://doi.org/10.1038/s41561-019-0334-6, 2019.

Ferrari, R., Jansen, M. F., Adkins, J. F., Burke, A., Stewart, A. L., and Thompson, A. F.: Antarctic sea ice control on ocean circulation in present and glacial climates, Proc. Natl. Acad. Sci. U.S.A., 111, 8753–8758, https://doi.org/10.1073/pnas.1323922111, 2014.

Ford, H. L. and Raymo, M. E.: Regional and global signals in seawater $\delta^{18}O$ records across the mid-Pleistocene transition, Geology, 48, 113–117, https://doi.org/10.1130/G46546.1, 2020.

Ford, H. L., Sosdian, S. M., Rosenthal, Y., and Raymo, M. E.: Gradual and abrupt changes during the Mid-Pleistocene Transition, Quat. Sci. Rev., 148, 222–233, https://doi.org/10.1016/j.quascirev.2016.07.005, 2016.

Frew, R. D., Dennis, P. F., Heywood, K. J., Meredith, M. P., and Boswell, S. M.: The oxygen isotope composition of water masses in the northern North Atlantic, Deep-Sea Res. Oceanogr. Res. Pap., 47, 2265–2286, https://doi /10.1016/S0967-0637(00)00023-6, 2000.

Ganopolski, A.: Toward generalized Milankovitch theory (GMT), Clim. Past, 20, 151–185, https://doi.org/10.5194/cp-20-151-2024, 2024.

Gildor, H. and Tziperman, E.: Physical mechanisms behind biogeochemical glacial-interglacial CO_2 variations, Geophys. Res. Lett., 28, 2421–2424, https://doi.org/org/10.1029/2000GL012571, 2001.

Grant, K. M., Rohling, E. J., Bar-Matthews, M., Ayalon, A., Medina-Elizalde, M., Ramsey, C. B., Satow, C., and Roberts, A. P.: Rapid coupling between ice volume and polar temperature over the past 150,000 years, Nature, 491, 744–747, https://doi.org/10.1038/nature11593, 2012.

Grant, K. M., Rohling, E. J., Bronk Ramsey, C., Cheng, H., Edwards, R. L., Florindo, F., Heslop, D., Marra, F., Roberts, A. P., Tamisiea, M. E., and Williams, F.: Sea-level variability over five glacial cycles, Nat. Commun., 5, https://doi.org/10.1038/ncomms6076, 2014.

Greaves, M. J.,: Trace Elements in Marine Biogenic Carbonates: Analysis and Application to Past Ocean Chemistry, Ph.D. thesis, University of Southampton 194 pp., 2008.

Greaves, M., Caillon, N., Rebaubier, H., Bartoli, G., Bohaty, S., Cacho, I., Clarke, L., Cooper, M., Daunt, C., Delaney, M., DeMenocal, P., Dutton, A., Eggins, S., Elderfield, H., Garbe-Schoenberg, D., Goddard, E., Green, D., Groeneveld, J., Hastings, D., Hathorne, E., Kimoto, K., Klinkhammer, G., Labeyrie, L., Lea, D. W., Marchitto, T., Martínez-Botí, M.

A., Mortyn, P. G., Ni, Y., Nuernberg, D., Paradis, G., Pena, L., Quinn, T., Rosenthal, Y., Russel, A., Sagawa, T., Sosdian, S., Stott, L., Tachikawa, K., Tappa, E., Thunell, R., and Wilson, P. A.: Interlaboratory comparison study of calibration standards for foraminiferal Mg/Ca thermometry, Geochem, Geophys. Geosyst., 9, 1–27, https://doi.org/10.1029/2008GC001974, 2008.

Grimmer, M., Baggenstos, D., Schmitt, J., Krauss, F., Shackleton, S., Severinghaus, J. P., and Fischer, H.: AMOC modulates ocean heat content during deglaciations, Geophys. Res. Lett., 52, 1–12, https://doi.org/10.1029/2024GL114415, 2025.

Hall, I. R., McCave, I. N., Shackleton, N. J., Weedon, G. P., and Harris, S. E.: Intensified deep Pacific inflow and ventilation in Pleistocene glacial times, Nature, 412, 809–812, https://doi.org/10.1038/35090552, 2001.

Hasenfratz, A. P., Martínez-García, A., Jaccard, S. L., Vance, D., Wälle, M., Greaves, M., and Haug, G. H.: Determination of the Mg/Mn ratio in foraminiferal coatings: An approach to correct Mg/Ca temperatures for Mn-rich contaminant phases, Earth Planet. Sci. Lett., 457, 335–347, https://doi.org/10.1016/j.epsl.2016.10.004, 2017.

Hasenfratz, A. P., Jaccard, S. L., Martínez-García, A., Sigman, D. M., Hodell, D. A., Vance, D., Bernasconi, S. M., Kleiven, H. (Kikki) F., Haumann, F. A., and Haug, G. H.: The residence time of Southern Ocean surface waters and the 100,000-year ice age cycle, Science, 363, 1080–1084, https://doi.org/10.1126/science.aat7067, 2019.

Herbert, T. D.: The Mid-Pleistocene Climate Transition, Annu. Rev. Earth Planet. Sci., 51, 389–418, https://doi.org/10.1146/annurev-earth-032320- 104209, 2023.

Higgins, J. A., Kurbatov, A. V., Spaulding, N. E., Brook, E., Introne, D. S., Chimiak, L. M., Yan, Y., Mayewski, P. A., and Bender, M. L.: Atmospheric composition 1 million years ago from blue ice in the Allan Hills, Antarctica, Proc. Natl. Acad. Sci., 112, 6887–6891, https://doi.org/10.1073/pnas.1420232112, 2015.

Hines, S. K. V., Charles, C. D., Starr, A., Goldstein, S. L., Hemming, S. R., Hall, I. R., Lathika, N., Passacantando, M., and Bolge, L.: Revisiting the mid-Pleistocene transition ocean circulation crisis, Science, 386, 681–686, https://doi.org/10.1126/science.adn4154, 2024.

Hodell, D. A., Elderfield, H., Greaves, M., McCave, I. N., Skinner, L., Thomas, A., White, N.: The JC089 scientific party, JC089 cruise report—IODP site survey of the Shackleton sites, SW Iberian Margin, British Oceanographic Data Centre, https://www.bodc.ac.uk/resources/inventories/cruise_inventory/report/13392/, 2014

Hodell, D., Lourens, L., Crowhurst, S., Konijnendijk, T., Tjallingii, R., Jimenez-Espejo, F., Skinner, L., and Tzedakis, P. C., Abrantes, F., Acton, G. D., Alvarez Zarikian, C. A., Bahr, A., Balestra, B., Barranco, E. L., Carrara, G., Ducassou, E., Flood, R. D., Flores, J.-A., Furota, S., Grimalt, J., Grunert, P., Hernandez- Molina, J., Kim, J. K., Krissek, L. A., Kuroda, J., Li, B., Lofi, J., Margari, V., Martrat, B., Miller, M. D., Nanayama, F., Nishida, N., Richter, C., Rodrigues, T., Rodríguez-Tovar, F. J., Roque, A. C. F., Sanchez Goni, M. F., Sierro Sanchez, F. J., Singh, A. D., Sloss, C. R., Stow, D. A., Takashimizu, Y., Tzanova, A., Voelker, A., Xuan, C., and Williams, T.: A reference time scale for Site U1385 (Shackleton Site) on the SW Iberian Margin, Glob. Planet. Change, 133, 49–64, https://doi.org/10.1016/j.gloplacha.2015.07.002, 2015.

Hodell, D. A., Venz, K. A., Charles, C. D., and Ninnemann, U. S.: Pleistocene vertical carbon isotope and carbonate gradients in the South Atlantic sector of the Southern Ocean, Geochem, Geophys. Geosyst., 4, 1–19, https://doi.org/10.1029/2002GC000367, 2003.

Hodell, D. A., Crowhurst, S., Lourens, L., Margari, V., Nicolson, J., Rolfe, J. E., Skinner, L. C., Thomas, N., Tzedakis, P. C., Mleneck-Vautravers, M. J., and Wolff, E. W.: A 1.5-million-year record of orbital and millennial climate variability in the North Atlantic, Clim. Past, 19, 607–636, https://doi.org/10.5194/cp-19-607-2023, 2023.

Hodell, D. A., Abrantes, F., Alvarez Zarikian, C. A., Herbert, T. D., Du, M., Crowhurst, S. J., Mleneck-Vautravers, M., Rolfe, J. E., Chen, X., Brooks, H. L., Clark, W. B., Dauchy-Tric, L. F. B., Dos Santos Rocha, V., Flores, J. A., Hines, S. K. V., Huang, H. H. M., Ikeda, H., Kaboth-Bahr, S., Kuroda, J., Link, J. M., McManus, J. F., Mitsunaga, B. A., Yobo, L. N., Pallone, C. T., Pang, X., Péral, M. Y., Salgueiro, E., Sanchez, S., Verma, K., Wu, J., Xuan, C., Yu, J., Haygood, L. A., Liebrand, D., Magalhães, V., Alonso-Garcia, M., Duque-Castaño, M., Ferreira, F., Freitas, M., Cordeiro, L. G., Gil, I., González-Martín, M., Lopes, A., Lopes, C., Margari, V., Martín-García, L., Matos, L., Mega, A., Molina, G., Naughton, F., Oliveira, D., Rebotim, A., Rodrigues, T., Santana, A., Trejos-Tamayo, R., and Tzedakis, P. C.: Onset of millennial climate variability with the intensification of Northern Hemisphere glaciation, Science, 392, 57–62, https://doi.org/10.1126/science.ady7970, 2026.

Hönisch, B., Hemming, N. G., Archer, D., Siddall, M., and McManus, J. F.: Atmospheric carbon dioxide concentration across the Mid-PleistoceneTransition, Science, 324, 1551–1554, https://doi.org/10.1126/science.1171477, 2009.

Imbrie, J., Hays, J. D., Martinson, D. G., McIntyre, A., Mix, A. C., Morley, J. J., Pisias, N. G., Prell, W. L., and Shackleton, N. J.: The orbital theory of Pleistocene climate: support from a revised chronology of the marine $\delta^{18}O$ record, in: Milankovitch and climate., Part 1, edited by: Berger, A. L. Imbrie, J., Hays, J., Kukla, G., Saltzman., Springer Dordrecht, 269–305, 1984.

Insua, T. L., Spivach, A. J., Graham, D., D'Hondt, S., and Moran, K.: Reconstruction of Pacific Ocean bottom water salinity during the Last Glacial Maximum, Geophys. Res. Lett., 41, 2914–2920, https://doi.org/10.1002/2014GL059575, 2014.

Jaccard, S. L., Hayes, C. T., Martínez-García, A., Hodell, D. A., Anderson, R. F., Sigman, D. M., and Haug, G. H.: Two modes of change in Southern Ocean productivity over the past million years, Science, 339, 1419–1423, https://doi.org/10.1126/science.1227545, 2013.

Jansen, M. F.: Glacial ocean circulation and stratification explained by reduced atmospheric temperature, Proc. Natl. Acad. Sci. U. S. A., 114, 45–50, https://doi.org/10.1073/pnas.1610438113, 2017.

Kim, H. and Timmermann, A.: Seawater oxygen isotopes as a tool for monitoring future meltwater from the Antarctic ice-sheet, Commun. Earth Environ., 5, 1–11, https://doi.org/10.1038/s43247-024-01514-4, 2024.

Kim, J., Goldstein, S. L., Pena, L. D., Jaume-Seguí, M., Knudson, K. P., Yehudai, M., and Bolge, L.: North Atlantic Deep Water during Pleistocene interglacials and glacials, Quat. Sci. Rev., 269, 1–19, https://doi.org/10.1016/j.quascirev.2021.107146, 2021.

Knorr, G., Barker, S., Zhang, X., Lohmann, G., Gong, X., Gierz, P., Stepanek, C., and Stap, L. B.: A salty deep ocean as a prerequisite for glacial termination, Nat. Geosci., 14, 930–936, https://doi.org/10.1038/s41561-021-00857-3, 2021.

Lamy, F., Winckler, G., Arz, H. W., Farmer, J. R., Gottschalk, J., Lembke-Jene, L., Middleton, J. L., van der Does, M., Tiedemann, R., Alvarez Zarikian, C., Basak, C., Brombacher, A., Dumm, L., Esper, O. M., Herbert, L. C., Iwasaki, S., Kreps, G., Lawson, V. J., Lo, L., Malinverno, E., Martinez-Garcia, A., Michel, E., Moretti, S., Moy, C. M., Ravelo, A. C., Riesselman, C. R., Saavedra-Pellitero, M., Sadatzki, H., Seo, I., Singh, R. K., Smith, R. A., Souza, A. L., Stoner, J. S., Toyos, M., de Oliveira, I. M. V. P., Wan, S., Wu, S., and Zhao, X.: Five million years of Antarctic Circumpolar Current strength variability, Nature, 627, 789–796, https://doi.org/10.1038/s41586-024-07143-3, 2024.

Lang, D. C., Bailey, I., Wilson, P. A., Chalk, T. B., Foster, G. L., and Gutjahr, M.: Incursions of southern-sourced water into the deep North Atlantic during late Pliocene glacial intensification, Nat. Geosci., 9, 375–379, https://doi.org/10.1038/ngeo2688, 2016.

de Lange, G. J., van Os, B., and Poorter, R.: Geochemical composition and inferred accretion rates of sediments and managanese nodules from a submarine hill in the Madeira Abyssal Plain, eastern North Atlantic, Mar. Geol., 109, 171–194, https://doi.org/10.1016/0025-3227(92)90227-9, 1992.

Larsson, V. and Jung, S.: Persistent contamination in benthic-foraminifera-based Mg/Ca thermometry using standard cleaning methods, Clim. Past, 21, 1871–1894, https://doi.org/10.5194/cp-21-1871-2025, 2025.

Lawrence, K. T., Herbert, T. D., Brown, C. M., Raymo, M. E., and Haywood, A. M.: High-amplitude variations in North Atlantic sea surface temperature during the early Pliocene warm period, Paleoceanography, 24, 1–15, https://doi.org/10.1029/2008PA001669, 2009.

Lear, C. H., Rosenthal, Y., and Wright, J. D.: The closing of a seaway: Ocean water masses and global climate change, Earth Planet. Sci. Lett., 210, 425–436, https://doi.org/10.1016/S0012-821X(03)00164-X, 2003.

Lear, C. H., Billups, K., Rickaby, R. E. M., Diester-Haass, L., Mawbey, E. M., and Sosdian, S. M.: Breathing more deeply: Deep ocean carbon storage during the mid-Pleistocene climate transition, Geology, 44, 1035–1038, https://doi.org/10.1130/G38636.1, 2016.

Legrain, E., Parrenin, F., and Capron, E.: A gradual change is more likely to have caused the Mid-Pleistocene Transition than an abrupt event, Commun. Earth Environ., 4, 1–10, 2023.

LeGrande, A. N. and Schmidt, G. A.: Global gridded data set of the oxygen isotopic composition in seawater, Geophys. Res. Lett., 33, L12604, https://doi.org/10.1029/2006GL026011, 2006.

Li, K., Tian, J., Zhao, N., Du, J., Liu, Z., Du, J., and Huang, E.: Stable Pacific deep circulation punctuated by episodic intensification during the Mid-Pleistocene Transition, Glob. Planet. Change, 257, https://doi.org/10.1016/j.gloplacha.2025.105229, 2026.

Lin, L., Khider, D., Lisiecki, L. E., and Lawrence, and C. E.: Probabilistic sequence alignment of stratigraphic records, Paleoceanography, 29, 976–989, https://doi.org/10.1002/2014PA002713, 2014.

Lisiecki, L. E.: Atlantic overturning responses to obliquity and precession over the last 3 Myr, Paleoceanography, 29, 71–86, https://doi.org/10.1002/2013PA002505, 2014.

Lisiecki, L. E. and Raymo, M. E.: A Pliocene-Pleistocene stack of 57 globally distributed benthic $\delta^{18}O$ records, Paleoceanography, 20, PA1003, https://doi.org/10.1029/2004PA001071, 2005.

Lisiecki, L. E. and Stern, J. V.: Regional and global benthic $\delta^{18}O$ stacks for the last glacial cycle, Paleoceanography, 31, 1368–1394, https://doi.org/10.1002/2016PA003002, 2016.

Marks-Peterson, J., Shackleton, S., Higgins, J., Severinghaus, J., Yan, Y., Buizert, C., Kalk, M., Beaudette, R., Hishamunda, V., Eves, D., Carter, A., Kurbatov, A., Epifanio, J., Morgan, J., Nesbitt, I., Bender, M., and Brook, E.: Broadly stable atmospheric CO_2 and CH_4 levels over the past 3 million years, Nature, 651, 647–651, https://doi.org/10.1038/s41586-025-10032-y, 2026.

Martínez-Garcia, A., Rosell-Melé, A., McClymont, E. L., Gersonde, R., and Haug, G. H.: Subpolar link to the emergence of the modern equatorial pacific cold tongue, Science, 328, 1550–1553, https://doi.org/10.1126/science.1184480, 2010.

Martínez-Garcia, A., Rosell-Melé, A., Jaccard, S. L., Geibert, W., Sigman, D. M., and Haug, G. H.: Southern Ocean dust-climate coupling over the past four million years, Nature, 476, 312–315, https://doi.org/10.1038/nature10310, 2011.

McClymont, E. L., Sosdian, S. M., Rosell-Melé, A., and Rosenthal, Y.: Pleistocene sea-surface temperature evolution: Early cooling, delayed glacial intensification, and implications for the mid-Pleistocene climate transition, Earth-Science Rev., 123, 173–193, https://doi.org/10.1016/j.earscirev.2013.04.006, 2013.

McKay, R., Naish, T., Powell, R., Barrett, P., Scherer, R., Talarico, F., Kyle, P., Monien, D., Kuhn, G., Jackolski, C., and Williams, T.: Pleistocene variability of Antarctic Ice Sheet extent in the Ross Embayment, Quat. Sci. Rev., 34, 93–112, https://doi.org/10.1016/j.quascirev.2011.12.012, 2012.

Oliveira, D., Desprat, S., Rodrigues, T., Naughton, F., Hodell, D., Trigo, R., Rufino, M., Lopes, C., Abrantes, F., and Sánchez Goñi, M. F.: The complexity of millennial-scale variability in southwestern Europe during MIS 11, Quat. Res. (United States), 86, 373–387, https://doi.org/10.1016/j.yqres.2016.09.002, 2016.

Pena, L. D. and Goldstein, S. L.: Thermohaline circulation crisis and impacts during the mid-Pleistocene transition, Science, 345, 318–322, https://doi.org/10.1126/science.1249770, 2014.

Peng, Z., Wang, R., Xiao, W., Jin, X., Dang, H., Ye, S., Wu, L., Wang, X., Liu, F., and Dang, S.: Sustained increase in Southwest Pacific Antarctic Intermediate Water carbon storage across the Mid-Pleistocene Transition, Glob. Planet. Change, 262, https://doi.org/10.1016/j.gloplacha.2026.105470, 2026.

Pérez-Montero, S., Alvarez-solas, J., Swierczek-Jereczek, J., Moreno-Parada, D., Robinson, A., and Montoya, M.: Exploring the Mid-Pleistocene transition with a simple physical model, Clim. Past, 22, 625–646, https://doi.org/10.5194/cp-22-625-2026, 2026.

Pisias, N. G. and Moore, T. C.: The evolution of Pleistocene climate: A timeseries approach, Earth Planet. Sci. Lett., 52, 450–458, https://doi.org/10.1016/0012-821X(81)90197-7, 1981.

Pöppelmeier, F., Blaser, P., Gutjahr, M., Jaccard, S. L., Frank, M., Max, L., and Lippold, J.: Northern-sourced water dominated the Atlantic Ocean during the Last Glacial Maximum, Geology, 48, 826–829, https://doi.org/10.1130/g47628.1, 2020.

Pöppelmeier, F., Lippold, J., Blaser, P., Gutjahr, M., Frank, M., and Stocker, T. F.: Neodymium isotopes as a paleo-water mass tracer: A model-data reassessment, Quat. Sci. Rev., 279, https://doi.org/10.1016/j.quascirev.2022.107404, 2022.

Qin, B., Jia, Q., Xiong, Z., Li, T., Algeo, T. J., and Dang, H.: Sustaineddeep Pacific carbon storage after the Mid-Pleistocene Transition linked to enhanced Southern Ocean stratification, Geophys. Res. Lett., 49, e2021GL097121, https://doi.org/10.1029/2021GL097121, 2022.

Raymo, M. E., Oppo, D. W., and Curry, W.: The mid-Pleistocene climate transition: A deep sea carbon isotopic perspective, Paleoceanography, 12, 546–559, https://doi.org/10.1029/97PA01019, 1997.

Raymo, M. E., Lisiecki, L. E., and Nisancioglu, K. H.: Plio-Pleistocene ice volume, Antarctic climate, and the global $\delta^{18}O$ record., Nature, 313, 492–495, https://doi.org/10.1126/science.1123296, 2006.

Rohling, E. J., Yu, J., Heslop, D., Foster, G. L., Opdyke, B., and Roberts, A. P.: Sea level and deep-sea temperature reconstructions suggest quasi-stable states and critical transitions over the past 40 million years, Sci. Adv., 7, 1–7, https://doi.org/10.1126/sciadv.abf5326, 2021.

Shackleton, N.: Oxygen Isotope Analyses and Pleistocene Temperatures Re-assessed, Nature, 215, 15–17, https://doi.org/10.1038/215015a0, 1967.

Shackleton, N. J.: The 100,000-year ice-age cycle identified and found to lag temperature, carbon dioxide, and orbital eccentricity, Science, 289, 1897–1902, https://doi.org/10.1126/science.289.5486.1897, 2000.

Shackleton, N. J. and Opdyke, N. D.: Oxygen isotope and palaeomagnetic stratigraphy of Equatorial Pacific core V28-238: Oxygen isotope temperatures and ice volumes on a 10^5 year and 10^6 year scale, Quat. Res., 3, 39–55,//dx.doi.org/10.1016/0033-5894(73)90052-5, 1973.

Shackleton, N. J. and Opdyke, N. D.: Oxygen-isotope and paleomagnetic stratigraphy of Pacific core V28-239 late Pliocene to latest Pleistocene, Mem. Geol. Soc. Am., 145, 449–464, https://doi.org/10.1130/MEM145-p449, 1976.

Shackleton, S., Seltzer, A., Baggenstos, D., and Lisiecki, L. E.: Benthic $\delta^{18}O$ records Earth's energy imbalance, Nat. Geosci., 16, 797–802, https://doi.org/10.1038/s41561-023-01250-y, 2023.

Shackleton, S., Hishamunda, V., Yan, Y., Carter, A., Morgan, J., Severinghaus, J., Aarons, S., Marks-Peterson, J., Epifanio, J., Buizert, C., Brook, E., Kurbatov, A. V., Bender, M. L., and Higgins, J.: Global ocean heat content over the past 3 million years, Nature, 651, 653–657, https://doi.org/10.1038/s41586-026-10116-3, 2026.

Siddall, M., Hönisch, B., Waelbroeck, C., and Huybers, P.: Changes in deep Pacific temperature during the mid-Pleistocene transition and Quaternary, Quat. Sci. Rev., 29, 170–181, https://doi.org/10.1016/j.quascirev.2009.05.011, 2010.

Sigman, D. M., Hain, M. P., and Haug, G. H.: The polar ocean and glacial cycles in atmospheric CO_2 concentration, Nature, 466, 47–55, https://doi.org/10.1038/nature09149, 2010.

Sigman, D. M., Fripiat, F., Studer, A. S., Kemeny, P. C., Martínez-García, A., Hain, M. P., Ai, X., Wang, X., Ren, H., and Haug, G. H.: The Southern Ocean during the ice ages: A review of the Antarctic surface isolation hypothesis, with comparison to the North Pacific, Quat. Sci. Rev., 254, 106732, https://doi.org/10.1016/j.quascirev.2020.106732, 2021.

Skinner, L. C. and Elderfield, H.: Rapid fluctuations in the deep North Atlantic heat budget during the last glacial period, Paleoceanography, 22, PA1205, https://doi.org/10.1029/2006PA001338, 2007.

Skinner, L. C., Shackleton, N. J., and Elderfield, H.: Millennial-scale variability of deep-water temperature and $\delta^{18}O_{dw}$ indicating deep-water source variations in the Northeast Atlantic, 0-34 cal. ka BP, Geochem, Geophys. Geosyst., 4, 1098, https://doi.org/10.1029/2003GC000585, 2003.

Skinner, L. C., Elderfield, H., and Hall, M.: Phasing of millennial climate events and Northeast Atlantic Deep-Water temperature change since 50 ka BP, in: Ocean Circulation: Mechanisms and Impacts—Past and Future Changes of Meridional Overturning, edited by: Schmittner, A., Chiang, J.C.H., and Hemming, S.R., American Geophysical Union 197–208, https://doi.org/10.1029/173GM14, 2007.

Song, Z., Latif, M., Park, W., and Zhang, Y.: Southern Ocean influence on Atlantic Meridional Overturning Circulation across climate states, Nat. Commun. , 16, https://doi.org/10.1038/s41467-025-64268-3, 2025.

Sosdian, S. and Rosenthal, Y.: Deep-sea temperature and ice volume changes across the Pliocene-Pleistocene climate transitions, Science, 325, 306–310, https://doi.org/10.1126/science.1169938, 2009.

Sosdian, S. and Rosenthal, Y.: Response to Comment on "Deep-sea temperature and ice volume changes across the Pliocene-Pleistocene climate transitions," Science, 328, https://doi.org/10.1126/science.1186768, 2010.

Starr, A., Hall, I., Barker, S., Rackow, T., Zhang, X., Hemming, S., van der Lubbe, H., Knorr, G., Berke, M., Bigg, G. R., Cartagena-Sierra, A., Jiménez-Espejo, F. J., Gong, X., Gruetzner, J., Lathika, N., LeVay, L. J., Robinson, R. S., and Ziegler, M.: Antarctic icebergs reorganise ocean circulation during Pleistocene glacials, Nature, 589, 236–241, https://doi.org/10.1038/s41586-020-03094-7, 2021.

Sun, S., Eisenman, I., and Stewart, A. L.: The influence of Southern Ocean surface buoyancy forcing on glacial-interglacial changes in the global deep ocean stratification, Geophys. Res. Lett., 43, 8124–8132, https://doi.org/10.1002/2016GL070058, 2016.

Talley, L. D.: Closure of the global overturning circulation through the Indian, Pacific, and Southern Oceans: Schematics and transports., Oceanography, 26, 80–97, https://doi.org/10.5670/oceanog.2013.07, 2013.

Thirumalai, K., Quinn, T. M., and Marino, G.: Constraining past seawater $\delta^{18}O$ and temperature records developed from foraminiferal geochemistry, Paleoceanography, 31, 1409–1422, https://doi.org/10.1002/2016PA002970, 2016.

Thomas, N. C., Bradbury, H. J., and Hodell, D. A.: Changes in North Atlantic deep-water oxygenation across the Middle Pleistocene Transition, Science, 377, 654–659, doi: 10.1126/science.abj7761, 2022.

Toyota, T., Smith, I. J., Gough, A. J., Langhorne, P. J., Leonard, G. H., Van Hale, R. J., Mahoney, A. R., and Haskell, T. G.: Oxygen isotope fractionation during the freezing of sea water, J. Glaciol., 59, 697–710, https://doi.org/10.3189/2013JoG12J163, 2013.

de Villiers, S., Greaves, M., and Elderfield, H.: An intensity ratio calibration method for the accurate determination of Mg/Ca and Sr/Ca of marine carbonates by ICP-AES, Geochem, Geophys. Geosyst., 3, https://doi.org/10.1029/2001GC000169, 2002.

Waelbroeck, C., Labeyrie, L., Michel, E., Duplessy, J. C., McManus, J. F., Lambeck, K., Balbon, E., and Labracherie, M.: Sea-level and deep water temperature changes derived from benthic foraminifera isotopic records, Quat. Sci. Rev., 21, 295–305, https://doi.org/10.1016/S0277-3791(01)00101-9, 2002.

Weldeab, S., Arce, A., and Kasten, S.: Mg/Ca-$\Delta CO^{2-}{}_{3\,\mathrm{pore\ water}}$-temperature calibration for *Globobulimina* spp.: A sensitive paleothermometer for deep-sea temperature reconstruction, Earth Planet. Sci. Lett., 438, 95–102, https://doi.org/10.1016/j.epsl.2016.01.009, 2016.

Willeit, M., Ganopolski, A., Calov, R., and Brovkin, V.: Mid-Pleistocene transition in glacial cycles explained by declining CO_2 and regolith removal, Sci. Adv., 5, 1–9, https://doi.org/10.1126/sciadv.aav7337, 2019.

Williams, T. J., Piotrowski, A. M., Howe, J. N. W., Hillenbrand, C-D., Allen, C. S., and Clegg, J. A.: The role of ocean circulation and regolith removal in triggering the Mid-Pleistocene Transition: Insights from authigenic Nd isotopes, Quat. Sci. Rev., 345, 109055, https://doi.org/10.1016/j.quascirev.2024.109055, 2024.

Wirths, C., Hermant, A., Stepanek, C., Stocker, T. F., and Sutter, J. C. R.: Sequence of abrupt transitions in Antarctic drainage basins before and during the Mid-Pleistocene Transition, Nat. Commun., 16, 10391, https://doi.org/10.1038/s41467-025-65375-x, 2025.

Wolff, E. W., Fischer, H., van Ommen, T., and Hodell, D. A.: Stratigraphic templates for ice core records of the past 1.5 Myr, Clim. Past, 18, 1563–1577, https://doi.org/10.5194/cp-18-1563-2022, 2022.

Wolff, E. W.: Surprises trapped in three-million-year-old ice, Nature, 651, 592–593, 2026.

Yan, Y., Bender, M. L., Brook, E. J., Clifford, H. M., Kemeny, P. C., Kurbatov, A. V., Mackay, S., Mayewski, P. A., Ng, J., Severinghaus, J. P., and Higgins, J. A.: Two-million-year-old snapshots of atmospheric gases from Antarctic ice, Nature, 574, 663–666, https://doi.org/10.1038/s41586-019-1692-3, 2019.

Yang, Z., Lear, C. H., Barker, S., Elsey, J., Gasson, E., Rosenthal, Y., Slater, S. M., and Thomas-Sparkes, A.: Major sea level fall during the Pliocene M2 glaciation, Nat. Commun., 16, 7641, https://doi.org/10.1038/s41467-025-62446-x, 2025.

Yehudai, M., Kim, J., Pena, L. D., Jaume-Segui, M., Knudson, K. P., Bolge, L., Malinverno, A., Bickert, T., and Goldstein, S. L.: Evidence for a Northern Hemispheric trigger of the 100,000-y glacial cyclicity, Proc. Natl. Acad. Sci. U. S. A., 118, https://doi.org/10.1073/pnas.2020260118, 2021.

Yu, J. and Broecker, W. S.: Comment on "Deep-sea temperature and ice volume changes across the Pliocene-Pleistocene Climate Transitions," Science, 328, 1480, https://doi.org/10.1126/science.1186544, 2010.

Zhao, N., Oppo, D. W., Huang, K. F., Howe, J. N. W., Blusztajn, J., and Keigwin, L. D.: Glacial–interglacial Nd isotope variability of North Atlantic Deep Water modulated by North American ice sheet, Nat. Commun., 10, 5773, https://doi.org/10.1038/s41467-019-13707-z, 2019.